Title:

Clumped isotopologue constraints on the origin of methane at seafloor hot springs

A revised manuscript prepared for submission to *Geochimica et Cosmochimica Acta* on 12 November 2017

Authors and affiliations:

David T. Wang[a,b,*], Eoghan P. Reeves[a,b,c], Jill M. McDermott[a,b,d], Jeffrey S. Seewald[b], and Shuhei Ono[a]

[a]Department of Earth, Atmospheric and Planetary Sciences, Massachusetts Institute of Technology, Cambridge, Massachusetts 02139, USA.
[b]Marine Chemistry and Geochemistry Department, Woods Hole Oceanographic Institution, Woods Hole, Massachusetts 02543, USA.
[c]Department of Earth Science and Centre for Geobiology, University of Bergen, Bergen N-5020, Norway.
[d]Earth and Environmental Sciences Department, Lehigh University, Bethlehem, Pennsylvania 18015, USA.

* Corresponding author. *E-mail address*: dtw@alum.mit.edu (D.T. Wang).

Keywords:
methane, hydrothermal vent fields, fluid inclusions, clumped isotopologues, hydrogen isotope exchange

Abstract

Hot-spring fluids emanating from deep-sea vents hosted in unsedimented ultramafic and mafic rock commonly contain high concentrations of methane. Multiple hypotheses have been proposed for the origin(s) of this methane, ranging from synthesis via reduction of aqueous inorganic carbon ($\sum CO_2$) during active fluid circulation to leaching of methane-rich fluid inclusions from plutonic rocks of the oceanic crust. To further resolve the process(es) responsible for methane generation in these systems, we determined the relative abundances of several methane isotopologues (including $^{13}CH_3D$, a "clumped" isotopologue containing two rare isotope substitutions) in hot-spring source fluids sampled from four geochemically-distinct hydrothermal vent fields (Rainbow, Von Damm, Lost City, and Lucky Strike).

Apparent equilibrium temperatures retrieved from methane clumped isotopologue analyses average 310^{+53}_{-42} °C, with no apparent relation to the wide range of fluid temperatures (96 to 370 °C) and chemical compositions (pH, $[H_2]$, $[\sum CO_2]$, $[CH_4]$) represented. Combined with very similar bulk stable isotope ratios ($^{13}C/^{12}C$ and D/H) of methane across the suite of hydrothermal fluids, all available geochemical and isotopic data suggest a common mechanism of methane generation at depth that is disconnected from active fluid circulation. Attainment of equilibrium amongst methane isotopologues at temperatures of ca. 270 to 360 °C is compatible with the thermodynamically-favorable reduction of CO_2 to CH_4 at temperatures at or below ca. 400 °C under redox conditions characterizing intrusive rocks derived from sub-ridge melts. Collectively, the observations support a model where methane-rich aqueous fluids, known to be trapped in rocks of the oceanic lithosphere, are liberated from host rocks during hydrothermal circulation and perhaps represent the major source of methane venting with thermal waters at unsedimented hydrothermal fields. The results also provide further evidence that water-rock reactions occurring at temperatures lower than 200 °C do not contribute significantly to the quantities of methane venting at mid-ocean ridge hot springs.

Abstract: 292 words

Main Text: 6608 words

1. INTRODUCTION

Dissolved methane (CH_4) is ubiquitous in hot-spring fluids emanating from submarine hydrothermal vents, and a potential carbon source for microbial communities living at and below the seafloor and in the water column. Constraining sources of carbon (C) and hydrogen (H) for the production of CH_4, as well as the depths, temperatures, and timescales at which CH_4 is generated in these hydrothermal systems, is critical for understanding the origin of this form of hydrothermal carbon. The abundance and isotopic composition of CH_4 has been reported for fluids venting at unsedimented mid-ocean ridges and off-axis locations (e.g., Welhan, 1988b, Charlou et al., 2002, McCollom and Seewald, 2007, Proskurowski et al., 2008, Cannat et al., 2010, Charlou et al., 2010, Proskurowski, 2010, McDermott, 2015, and McDermott et al., 2015). In general, fluids that have interacted with ultramafic rock (peridotite and serpentinite) are enriched in CH_4 by one or more orders of magnitude relative to fluids that have reacted with mafic rock (basalt and gabbro) (Keir, 2010), although there are exceptions where high-CH_4 fluids emerge from mafic rock (Charlou et al., 2000).

Several distinct geochemical processes have been proposed to account for the presence of abiotic CH_4 in submarine hydrothermal fluids. Some have proposed that CH_4 is formed by reduction of aqueous inorganic carbon (i.e., $\sum CO_2$) during convective circulation of seawater-derived hydrothermal fluids in response to the highly reducing conditions that result from alteration of ultramafic rock (serpentinization) (Charlou et al., 2002; Proskurowski et al., 2008). Water-rock reactions during alteration of mafic rocks can also create sufficiently reducing conditions to reduce CO_2 to CH_4 without serpentinization (Shock, 1990; Seyfried and Ding, 1995), and is a possible source of the low but significant CH_4 observed in mafic-hosted systems (Keir, 2010). Others propose models involving entrapment and respeciation of mantle-derived CO_2 to CH_4 (and possibly to graphite) within plutonic (gabbroic) rocks of the oceanic crust (Kelley, 1996; Kelley, 1997; Kelley and Früh-Green, 1999), and subsequent extraction of the CH_4-rich trapped fluids during hydrothermal circulation (McDermott et al., 2015). Leaching of basalt-hosted gas vesicles that contain CH_4 may also be a source of CH_4 in fluids venting at fast-spreading ridges such as the East Pacific Rise (Welhan and Craig, 1983; Welhan, 1988a).

To constrain the origin of CH_4 in unsedimented submarine hydrothermal systems, we determined the relative abundance of four of its stable isotopologues ($^{12}CH_4$, $^{13}CH_4$, $^{12}CH_3D$, and $^{13}CH_3D$, a doubly-substituted or "clumped" isotopologue) in nine fluid samples collected from four hydrothermal vent fields: Rainbow (36°13'48" N, 33°54'09" W, Mid-Atlantic Ridge), Von Damm (18°22'36" N, 81°47'54" W, Mid-Cayman Rise), Lost City (30°07'24" N, 42°07'12" W, Mid-Atlantic Ridge), and Lucky Strike (37°17'30" N, 32°16'42" W, Mid-Atlantic Ridge). These fields span a wide range of vent temperatures (96 to 370 °C), represent distinct geological settings, and are characterized by a wide range of fluid compositions.

Data presented in this study provide constraints on the sources of C and H, as well as temperature(s) associated with the formation or equilibration of C–H bonds in CH_4 carried by fluids of the hot-spring source. Bulk carbon- and hydrogen-isotope ratios ($^{13}C/^{12}C$ and D/H) encode signals related to the sources of C and H, respectively, as well as isotopic fractionations incurred during the synthesis of CH_4. Complementary to such information, measurement of the CH_4 clumped isotopologue $^{13}CH_3D$ provides an independent estimate of the temperature at which the C–H bonds in CH_4 were formed or last equilibrated (Stolper et al., 2014; Wang et al., 2015). Constraining the temperatures at which CH_4 synthesis occurs within oceanic crust has direct implications for the distribution and availability of reduced carbon substrates and energy sources that may support a deep biosphere, as well as for the transfer of mantle-derived carbon to Earth's surface.

Determination of temperatures from bulk carbon or hydrogen isotope ratios of CH_4 alone requires knowledge of or assumptions regarding the isotopic composition of other species with which CH_4 has exchanged atoms (e.g., CO_2 or H_2O). In contrast, temperatures determined from the abundance of $^{13}CH_3D$ do not require information regarding such coexisting species. Thus, clumped isotopologue data in conjunction with bulk $^{13}C/^{12}C$ and D/H isotope ratios of CH_4 can be used to constrain the isotopic compositions of C- and H-bearing species associated with the CH_4 source when independent constraints are unavailable.[1] In the following discussion, we show how clumped isotopologue temperatures of CH_4, together with bulk $^{13}C/^{12}C$ and D/H isotope ratios, fluid chemistry, and thermodynamic considerations, indicate that CH_4 in unsedimented hydrothermal systems originates at temperatures in excess of 270 °C and constrain possible environments of methane generation.

2. METHODS

2.1. Vent fluid samples

The fluid samples studied herein were collected by ROV *Jason II* using isobaric gas-tight samplers (Seewald et al., 2002) during cruises to the Mid-Atlantic Ridge in 2008 (Reeves et al., 2014) and Mid-Cayman Rise in 2012 (McDermott et al., 2015). Subsamples of vent fluids extracted from the samplers were stored in pre-evacuated serum vials sealed with blue butyl rubber stoppers that were preconditioned by boiling in 2 M NaOH for 2–4 hours and rinsed in deionized water. When necessary, sample aliquots in multiple serum vials were combined ("pooled") prior to purification to obtain enough CH_4 for clumped isotopologue analysis (>1 cm^3 SATP). When possible, aliquots from the same fluid sampler were used. In some cases, however, it was necessary to combine aliquots from duplicate samples collected in separate samplers deployed in the same hydrothermal fluid during a submersible dive (Table 1). Due to the exceedingly low concentration of dissolved CH_4 in ambient bottom seawater ($<10^{-8}$ M, McDermott et al., 2015; Reeves et al., 2014) relative to concentrations in endmember vent fluids (samples regressed to zero Mg content) (Table 2), inadvertent entrainment of seawater during fluid collection has no measurable effect on the isotopic composition of CH_4 derived from vent fluids that was measured in this study.

2.2. Analytical techniques

Samples of CH_4 were purified via cryofocusing–preparative gas chromatography (Wang et al., 2015). The relative abundances of the methane stable isotopologues $^{12}CH_4$, $^{13}CH_4$, $^{12}CH_3D$, and $^{13}CH_3D$ were measured using a tunable infrared laser direct absorption spectroscopy technique described previously (Ono et al., 2014; Wang et al., 2015). Due to the small amounts of CH_4 (ca. 1 cm^3 STP) in samples analyzed as part of this study, a cold trap system was employed to recover and recycle gas samples for re-analysis (Wang et al., 2015). A set of samples for which isotopologue ratios had been previously determined was also re-measured using this recycling technique, to verify accuracy (Supplementary Table 1).

The abundance of $^{13}CH_3D$ relative to a random distribution of isotopes among the isotopologues (stochastic distribution) is tracked using the metric $\Delta^{13}CH_3D$, which is defined as: $\Delta^{13}CH_3D = \ln Q$ (or nearly equivalently, $Q - 1$), where Q is the reaction quotient of the isotope exchange reaction:

$$^{13}CH_4 + {}^{12}CH_3D \rightleftharpoons {}^{13}CH_3D + {}^{12}CH_4. \quad (1)$$

[1] This is analogous to using carbonate clumped isotope abundances to solve for the $^{18}O/^{16}O$ ratio of H_2O from which the carbonate precipitated. Readers are referred to Eiler (2007) for further information.

Values of $\Delta^{13}CH_3D > 0$‰ are used to calculate apparent equilibrium temperatures (T_{13D}) using the calibration of Wang et al. (2015), which is based on quantum chemical predictions for CH_4 isotopologues in the gas phase and anchored by measurements of methane samples heated in the presence of platinum catalyst at temperatures between 150 and 400 °C (Wang et al., 2015).

Bulk isotope values are reported herein using standard delta-notation, i.e., $\delta^{13}C = (^{13}C/^{12}C)_{sample}/(^{13}C/^{12}C)_{VPDB} - 1$, and $\delta D = (D/H)_{sample}/(D/H)_{VSMOW} - 1$. The permil (‰) symbol represents multiplication by 10^{-3}; hence, we have omitted the factor of 1000 commonly seen in definitions of δ and other isotope values. The $\delta^{13}C$ and δD values are calibrated against community reference gases NGS-1 and NGS-3 (Wang et al., 2015).

3. RESULTS

Results of stable carbon ($^{13}C/^{12}C$) and hydrogen (D/H) isotope ratio measurements are shown in Table 1. These results are in general agreement with previously-published CH_4 isotopic data for these samples or systems (Proskurowski et al., 2008; Charlou et al., 2010; Pester et al., 2012; McDermott et al., 2015). For fluids for which direct comparisons to literature data are possible, the $\delta^{13}C$ values of CH_4 we report in Table 1 are typically <0.5‰ different from those previously published. The largest deviation is a consistent 0.9‰ offset for all three samples from Von Damm compared to the published report of McDermott et al. (2015) that likely stems from a difference in calibration between the laboratories. Data for δD are sparse, but the δD value shown in Table 1 for Beehive vent at Lost City is identical to that previously reported (−127 ± 6‰; Proskurowski et al., 2008).

Similar isotopic values were observed across the different hydrothermal fields, ranging from −18‰ to −11‰ in $\delta^{13}C$ and −127‰ to −98‰ in δD. Variation between vents in the same field (generally <1‰ in both $\delta^{13}C$ and δD) is significantly smaller than variation across different fields. The consistency of stable isotope data of CH_4 within each field is added evidence for the interpretations previously drawn of conservative mixing of CH_4 between bottom seawater and a single CH_4-bearing endmember fluid at Rainbow (Charlou et al., 2002) and Von Damm (McDermott et al., 2015). A common source fluid has also been suggested for Lucky Strike (Pester et al., 2012) and Lost City (Seyfried et al., 2015) based on the compositions of fluids there.

Also shown in Table 1 are results of CH_4 clumped isotopologue analyses. All samples yielded values of $\Delta^{13}CH_3D > 0$‰, from which apparent equilibrium temperatures can be derived (Fig. 1C and Table 1). The unweighted mean of the $\Delta^{13}CH_3D$ values across all nine vent fluids studied is 1.57 ± 0.28‰ (standard deviation, 1*s*), corresponding to a $\Delta^{13}CH_3D$ temperature of 310^{+53}_{-42} °C (derived from projection of measured $\Delta^{13}CH_3D$ values onto the green curve in Fig. 1C). Data for individual vent fluids are analytically indistinguishable from this narrow range (Fig. 2B).

4. DISCUSSION

4.1. Closure temperatures for hydrogen exchange amongst CH_4, H_2, and H_2O in hydrothermal systems

The narrow range of measured $\Delta^{13}CH_3D$ values (averaging 1.57 ± 0.28‰, 1*s*) and corresponding apparent equilibrium temperatures for Reaction 1 of 310^{+53}_{-42} °C contrasts with the wide range of fluid temperatures (96 to 370°C) measured at the vents (Fig. 1, Table 2). Had the methane in these samples attained isotopologue equilibrium at measured vent temperatures, $\Delta^{13}CH_3D$ values from 4.0 to 1.3‰ would be expected, respectively. The observed range of clumped isotopologue data is much smaller than this predicted range (Fig. 1C), with $\Delta^{13}CH_3D$ temperatures generally equal to or higher than fluid temperatures (Fig. 2B). The clumped isotopologue data indicate that the bulk of CH_4 at the sites studied were either formed at or around 310 °C, or that CH_4 was generated elsewhere in the hydrothermal system (perhaps at lower or higher temperatures) with subsequent establishment of equilibrium amongst the CH_4 isotopologues at 270 to 360 °C.

In addition to clumped isotopologues, bulk hydrogen isotope abundances also yield temperature constraints. Isotopic exchange of D/H amongst H_2O, H_2, and CH_4 can be described by the following equilibria:

$$CH_4 + HDO \rightleftharpoons CH_3D + H_2O \tag{2}$$

$$H_2 + HDO \rightleftharpoons HD + H_2O \tag{3}$$

$$CH_3D + H_2 \rightleftharpoons CH_4 + HD \tag{4}$$

Each of these reactions is characterized by a temperature-dependent equilibrium constant, such that differences in the measured hydrogen isotopic ratios between CH_4–H_2O, H_2–H_2O, or H_2–CH_4 pairs can, in principle, be used to calculate apparent equilibrium temperatures for the respective reactions. Seafloor hydrothermal fluids have δD values of H_2O very close to 0‰ (i.e., seawater; Shanks et al., 1995; see Supplementary Table 2), such that differences in calculated isotopic temperatures between samples are almost entirely due to variations in δD values of CH_4 or H_2.

Equilibrium fractionation factors between dissolved H_2 and CH_4 and liquid H_2O are shown in Fig. 3 (blue and red curves, respectively). The fractionation factor for Reaction 3 (blue curves) was derived for each temperature by multiplying experimental fractionation factors for $H_2(g)/H_2O(g)$ of either Suess (1949) (thin solid line), Cerrai et al. (1954) (thick solid line), or Bardo and Wolfsberg (1976) (dashed line), by that for $H_2O(g)/H_2O(l)$ from Horita and Wesolowski's (1994) calibration.[2] The fractionation factor for Reaction 2 (red curves) was then obtained by multiplying the fractionation factors for Reaction 3 by the experimentally-calibrated $CH_4(g)/H_2(g)$ fractionation factor from Horibe and Craig (1995). Isotope effects of solvation were ignored because they are small (Muccitelli and Wen, 1978; Bacsik et al., 2002).

Figure 3 shows a compilation of reported δD values of CH_4 at hydrothermal vent fields free of sediment influence. All δD data of CH_4 from endmember fluids cluster around −110‰ ± 12‰ ($1s$), and are consistent with CH_4 having approached hydrogen isotopic equilibrium with seawater-like H_2O at temperatures in excess of 270 °C. An upper temperature limit cannot be specified because of uncertainty in where the true D/H equilibrium fractionation between CH_4 and H_2O lies, and the low sensitivity of D/H thermometry of CH_4–H_2O (see Fig. 3). Temperatures derived from $\Delta^{13}CH_3D$ data are also in the range of 270 to 360 °C (shown by arrows), indicating that in seafloor hydrothermal systems, hydrogen exchange amongst CH_4 isotopologues is accompanied by or proceeds through apparent hydrogen exchange between CH_4 and H_2O. Stated another way, Reaction 1 probably does not proceed as an elementary reaction in nature. Instead, Reaction 1 likely evolves towards a state of equilibrium indirectly as a consequence of other isotope exchange reactions such as that between CH_4 and H_2O (Reaction 2). Reactions 1 and 2 therefore appear to proceed at similar rates, and closure temperatures[3] for both reactions are

[2] Rolston et al. (1976) performed an experimental calibration of $H_2(g)/H_2O(l)$ from 0 to 100 °C. The Rolston et al. curve is not shown in Fig. 3 because it covers only a portion of the temperature range of interest, but would plot very close to the dashed blue curve representing Bardo and Wolfsberg (1976) × Horita and Wesolowski (1994).

[3] The *closure temperature* is the temperature below which isotopic values become "frozen" over observable time. Closure temperature is a function of cooling rate.

between 270 and 360 °C in hydrothermal systems. Below the closure temperature, processes that break and form C–H bonds in CH_4 are slower than rates characterizing subsurface cooling of hydrothermal fluids.

Isotope data for H_2 are also shown in Fig. 3. Unlike for CH_4, H_2 is characterized by large spread in δD values across sites (−700‰ to −330‰). Values for δD of H_2 strongly vary with measured vent temperature, with endmember fluids plotting very near the equilibrium curves. This indicates that H_2 exchanges H with H_2O at rates that keep pace with cooling of sub-seafloor fluids during ascent, and that the closure temperature for Reaction 3 is much lower than that for CH_4–H_2O. An estimation based on data from low-temperature vents places the closure temperature for abiotic H_2–H_2O exchange between 70 and 110 °C (gray arrows), albeit with large uncertainty. Rapid metabolic cycling of H_2 by microorganisms living at the vents may enable H_2–H_2O exchange to occur down to even lower temperatures (Proskurowski et al., 2006; Kawagucci et al., 2010).

The data also yield constraints on the kinetics of H_2–CH_4 exchange (Reaction 4). Figure 3 again shows that δD values of H_2 plot very close to H_2–H_2O equilibrium while δD values of CH_4 plot away from the CH_4–H_2O line below ~300 °C. This indicates that the closure temperature for H_2–CH_4 exchange must be high, probably not much lower than 270 °C. If H_2–CH_4 were to actually close at a low temperature (100 °C for example), δD values of CH_4 would instead plot close to the red curves because CH_4 would always be exchanging H with a population of H_2 molecules that has a fixed δD value at each temperature (because of rapid exchange kinetics for H_2–H_2O and a near-infinite pool of H in H_2O) shown by the blue curves. Indeed, experiments conducted with gas-phase reactants between 25 and 400 °C show that rates for Reaction 3 (H_2–H_2O) are 20 to 100 times faster than that of Reaction 4 (H_2–CH_4) given identical partial pressures of H_2 (Lécluse and Robert, 1994). It is possible that the apparent exchange of hydrogen between CH_4 and H_2O at ~300 °C discussed in preceding paragraphs actually proceeds through H_2 (i.e., both CH_4 and H_2O undergo D/H exchange with H_2, while not interacting directly with each other). If this is true, higher concentrations of H_2 would not only result in faster rates of H_2–CH_4 exchange, but would also accelerate exchange between CH_4 and H_2O assuming rates of forward and backwards reactions in Reaction 4 are first-order in both [H_2] and [CH_4].

The temperature-dependence of D/H exchange rates between CH_4, H_2, and liquid H_2O has been the subject of limited experimental study. Figure 4 summarizes the available experimental constraints for H_2–H_2O and CH_4–H_2O exchange. Experiments with H_2 in the presence of liquid H_2O showed no observable exchange over 40 days at 26 °C (Campbell et al., 2009), but yielded half-exchange timescales as short as 10 min at 225 °C (Hall et al., 1934; Lyon and Hulston, 1984). (The 225 °C experiments were conducted in the presence of potentially-catalytic metal surfaces, and may therefore overestimate rates of exchange compared to nature.) Lécluse and Robert (1994) reported second-order rate coefficients for isotope exchange between H_2 and H_2O in gas phase from 25 to 435 °C. To estimate exchange kinetics in liquid phase, we multiplied these second-order rate coefficients by the vapor pressure of pure H_2O at each temperature, calculated at 1000 bar using a subroutine of the R package CHNOSZ (Dick et al., 2008) from data of Johnson et al. (1992) and Wagner and Pruß (2002). The plotted relationship (the blue curve in Fig. 4) is consistent with calculations by Lin et al. (2005) who used data from the same study, but experimental investigation is necessary to confirm that the kinetics of exchange for H_2 dissolved in water are accurately represented.

Experiments on exchange between CH_4 and liquid H_2O are even scarcer, but available data suggest that half-exchange timescales are on the order of 10 to 100 years at 300 °C, and ~10,000 years at 240 °C (Fig. 4; Supplementary Fig. 1; Koepp, 1978; Reeves et al., 2012). These numbers have large uncertainties because data collected at very low extents of exchange must be extrapolated to obtain rate estimates. It is also not known how factors such as pH, redox state, minerals, or concentrations of sulfur, H_2, or carbon species might affect hydrogen exchange rates. Nevertheless, experiments and observations demonstrate that CH_4–H_2O exchange is at least several orders of magnitude slower than H_2–H_2O exchange.

4.2. Constraints on the origin of methane at seafloor hot springs

4.2.1. Evaluating potential microbial and thermogenic sources at unsedimented sites

A remaining question is whether CH_4 from the four vent fields we studied might be (*i*) thermogenic methane generated at >270 °C, or (*ii*) thermogenic or microbial methane generated during recharge at lower temperatures and later heated during hydrothermal circulation through deeper hotter root zones. Bulk δD or $\Delta^{13}CH_3D$ data may not answer the second question since all C–H (and C–D) bonds rearrange upon heating to >270 °C, and thus C–H bonds of CH_4 carry no information prior to heating above (and cooling below) ~270 °C. However, other data help to exclude microbial and thermogenic sources as significant.

Bulk $\delta^{13}C$ values of CH_4 fall within a relatively narrow range (−18‰ to −11‰) across fluids from all four unsedimented hydrothermal fields studied (Fig. 1A). Because the four sites we studied lack appreciable sedimentation, sedimentary organic carbon from which thermogenic hydrocarbons can be generated is in scarce supply (Welhan, 1988b; Reeves et al., 2014). Dissolved organic carbon in recharging seawater is a potential source of thermogenic methane, but can only account for ~40 μM (Sharp et al., 1995). In contrast, production of thermogenic methane by decomposition of organic matter at elevated temperatures is well documented from sediment-influenced vent sites such as Guaymas Basin (Welhan and Lupton, 1987; Simoneit et al., 1988) and Middle Valley (Cruse and Seewald, 2006). Methane from those sites are characterized by their low $\delta^{13}C$ values (−40 to −55‰) and high C_{2+} alkane concentrations (typical C_1/C_2 ratios <300), which are very different from the unsedimented fields ($\delta^{13}C > -24‰$ and C_1/C_2 >1000) (McCollom and Seewald, 2007).

Methane from a CH_4-rich (~60 mM; Reeves et al., 2014) endmember fluid venting at 299 °C in Guaymas Basin carried a $\Delta^{13}CH_3D$ temperature of 326^{+170}_{-95} °C (95% confidence interval) (Wang et al., 2015). This sample also had a δD value of CH_4 (−106‰) that is again consistent with hydrogen isotope equilibrium at ca. 300 °C with water of VSMOW-like composition (large yellow octagon in Fig. 5).[4] The similarity in δD and $\Delta^{13}CH_3D$ values of CH_4 between the sediment-influenced fluids and those from unsedimented fields, despite very different $\delta^{13}C$ of CH_4 (−44‰) and C_{2+} concentrations (McCollom and Seewald, 2007), suggests that at Guaymas Basin and other high-temperature sediment-influenced fields (Kawagucci et al., 2013; Douglas et al., 2017), hydrogen isotopes of CH_4 have also been reset by exchange with H_2O (and/or with H_2). We note that thermogenic natural gases generated at an early stage of kerogen maturation probably inherit C–H bonds from precursor organic molecules that have undergone hydrogen exchange with other organics (instead of with water) in water-poor source rocks prior to natural gas generation (Stolper et al., 2014; Wang, 2017). The latter CH_4 gases evolve towards apparent D/H equilibrium with water with increasing maturity (shown by the brown arrow in Fig. 5) (Clayton, 2003), perhaps by inheritance of H from methyl moieties that have previously exchanged with water (Hoering, 1984; Smith et al., 1985; Lewan, 1997; Schimmelmann et al., 1999; Schimmelmann et al., 2001; Seewald, 2003; Lis et al., 2006;

[4] *Note added in revision:* Methane clumped isotope data have now been reported from two additional seafloor hot-spring fluids. The samples are from the Main Endeavour field on the Juan de Fuca Ridge (Douglas et al., 2017). These fluids have elevated concentrations of CH_4 (millimolar) and low $\delta^{13}C$ values (ca. −50‰), indicating the presence of buried and heated sedimentary organic matter that contributes thermogenic CH_4 (Lilley et al., 1993). The CH_4 is relatively enriched in deuterium (ca. −100‰) and carry high clumped isotope temperatures (~300 to 360 °C). These values are very similar to the Guaymas Basin sample from Wang et al. (2015) (see Fig. 5), providing additional evidence that apparent hydrogen-exchange occurs in high-temperature fluids from sediment-influenced fields.

Schimmelmann et al., 2006; Reeves et al., 2012; Wang, 2017), or in the case of the hot Guaymas Basin fluids, possible direct exchange of hydrogen between CH_4 and H_2O.

Microbial methane is generally characterized by low $\delta^{13}C$ values (<−60‰) due to carbon isotope fractionation during microbial methanogenesis. The methane $\delta^{13}C$ data alone, however, do not unambiguously exclude contributions of microbial methanogenesis, because high methane $\delta^{13}C$ values could be a result of near-quantitative conversion of $\sum CO_2$ to CH_4, particularly under $\sum CO_2$-limited conditions such as those present at Lost City (Brazelton et al., 2006; Bradley and Summons, 2010). Moreover, Takai et al. (2008) reported that carbon isotope fractionation by methanogens utilizing $\sum CO_2$ at >120 °C becomes very small (<12‰) under high H_2 partial pressure (150 bar), suggesting that microbially-derived CH_4 might have similar $\delta^{13}C$ values as those observed in unsedimented vent fluids (ca. 10 to 20‰ lower than seawater $\sum CO_2$, Fig. 1A). However, radiocarbon (^{14}C) abundances in CH_4 from Lost City and Von Damm are very low [fraction modern (F_m) averaging 0.004–0.006, near the limit of detection (F_m ~ 0.003)] (Proskurowski et al., 2008; McDermott et al., 2015), whereas ^{14}C contents of endmember $\sum CO_2$ at Von Damm are ~5× higher (McDermott et al., 2015). Had CH_4 been derived from reduction of $\sum CO_2$, the younger ^{14}C age of the $\sum CO_2$ would have been transferred to the CH_4 product. McDermott et al. (2015) further showed that $\sum CO_2$ in the vent fluids at Von Damm is likely seawater-derived, because both concentrations and $\delta^{13}C$ values of endmember $\sum CO_2$ match those of local bottom seawater. The conservation of $\sum CO_2$ during convective circulation at Von Damm excludes any process—microbial or otherwise—that converts $\sum CO_2$ in recharging seawater at Von Damm to CH_4 despite high energetic favorability for CH_4 synthesis at *in situ* conditions (Fig. 6D). The similarity in isotopic data and C_1/C_2 concentration values across the multiple vent fields studied here suggests that processes responsible for CH_4 generation at Von Damm are also occurring at the other unsedimented sites, even if the predominant influences on bulk fluid chemistry differ between sites. Therefore, the data described above support the idea that the endmember-derived CH_4 in the studied hydrothermal fluids is of dominantly abiotic origin (e.g., Charlou et al., 2002, McDermott et al., 2015, Proskurowski et al., 2008, and Welhan, 1988), and that the contribution of thermogenic or microbial processes to the CH_4 content of the endmember source component of fluids venting at each site is limited or insignificant.

4.2.2. High temperature origin of CH_4 at Lost City

The isotopologue data discussed above indicate that at Rainbow, Lucky Strike, Von Damm, and Lost City, CH_4 experienced temperatures in excess of 310^{+53}_{-42} °C at least once in its lifetime. The same processes responsible for the rupturing and healing of C–H bonds by which CH_4 isotopologues attain equilibrium may also drive concentrations of CH_4 to thermodynamic equilibrium. This is because the rate-limiting step for conversion of $\sum CO_2$ to/from CH_4 in hydrothermal fluids is thought to be the conversion of methanol (CH_3OH) to/from CH_4 (i.e., the formation/breakage of C–H bonds in CH_4) (Seewald et al., 2006; McCollom and Seewald, 2007; Reeves, 2010). Thus, $\Delta^{13}CH_3D$ and δD values of CH_4 likely record the most recent temperature at which CH_4 synthesis was both thermodynamically favorable and kinetically facile. This means that either net synthesis of CH_4 occurred at or above ca. 300 °C, or that CH_4 already existed and re-equilibrated at this temperature under conditions where CH_4 synthesis would have proceeded had there been $\sum CO_2$ available.

The $\Delta^{13}CH_3D$ temperature of 270^{+104}_{-68} °C we obtained for the Beehive vent fluid at Lost City argues for a much higher temperature of last exchange for the C–H bonds in methane than Proskurowski et al.'s (2006) suggestion of 110 to 150 °C. Their conclusion was based on hydrogen-isotope geothermometry of H_2–CH_4, and was premised on the assumption that δD values of H_2 and CH_4 in the Lost City vent fluids reflect isotope equilibrium between these species. However, as discussed earlier, rapid H_2–H_2O equilibration at temperatures lower than the closure (quench) temperatures for CH_4–H_2O or H_2–CH_4 exchange will shift δD values for H_2 progressively lower, while δD values of CH_4 remain unchanged. The fact that apparent temperatures derived from H_2–CH_4 will always be close to that from H_2–H_2O is a coincidence that results from equilibrium δD values for CH_4 being so poorly sensitive to temperature in comparison to those of H_2 (Fig. 3). Our $\Delta^{13}CH_3D$ data therefore suggest that at the most recent point at which CH_4 at Lost City was at isotopic equilibrium, surrounding temperatures were in excess of 200 °C, an assertion that is also supported by the bulk δD values of CH_4. The high methane clumped isotopologue temperature does not imply that the relatively cool fluids that vent at the surface today at Lost City experienced such high temperatures, because CH_4 may have been formed elsewhere and been entrained into cooler circulating fluids prior to their ascent to the seafloor (see Sec. 4.2.3).

4.2.3. A deep origin of methane disconnected from actively circulating fluids

The reduction of $\sum CO_2$ to CH_4 under hydrothermal conditions can be described by:

$$CO_2(aq) + 4H_2(aq) \rightleftharpoons CH_4(aq) + 2H_2O(l) \qquad (5)$$

Reduction of CO_2 is favored at temperatures below ~300 °C under redox conditions near the pyrite-pyrrhotite-magnetite (PPM) redox buffer, which approximates typical conditions for hydrothermal vent systems (Fig. 2A) (Shock, 1992; Seyfried and Ding, 1995). At sites with ultramafic rocks, reactions involved in the hydration of mafic minerals (serpentinization) can produce highly reducing conditions (H_2 fugacity more than 100-fold higher than PPM, Fig. 2). Serpentinization occurs at temperatures below 400 °C, where ferrous iron-bearing olivine and orthopyroxene minerals become unstable, with the highest H_2 fugacities produced at temperatures of 300 to 330 °C during serpentinization of peridotite under low water-to-rock ratios (Sleep et al., 2004; Klein et al., 2009; Klein et al., 2013). This range of temperatures is generally consistent with the closure temperatures indicated by our $\Delta^{13}CH_3D$ data, suggesting that formation of CH_4 probably did not occur at temperatures much higher than ca. 400 °C (Fig. 2B). However, while $\sum CO_2$ reduction (Reaction 5) is thermodynamically favorable under conditions encountered at ultramafic-hosted vents (Fig. 6D), the rate of the reaction is slow even at high temperatures (~300 °C). Numerous long-term experiments conducted between 177 and 325 °C with ^{13}C-labeled $\sum CO_2$ show that production of CH_4 is kinetically-hindered in the absence of metal catalysts such as native iron (McCollom and Seewald, 2001; McCollom and Seewald, 2003; Seewald et al., 2006; Reeves, 2010; McCollom, 2016; Grozeva et al., 2017). In most of these experiments, uncatalyzed rates of $\sum CO_2$ conversion of less than a few percent per year are observed. Considering that estimated residence times of fluids in the high-temperature reaction zone (>200 °C) of several mid-ocean ridge systems is years to decades (Kadko, 1996; Fisher, 2003), reduction of $\sum CO_2$ to CH_4 within actively-circulating hydrothermal fluids may be quite limited. Indeed, the isotopic composition and abundance of aqueous carbon species at the Von Damm vent field indicate that $\sum CO_2$ reduction to CH_4 is not occurring on the timescale of convective hydrothermal circulation there (see Sec. 4.2.1 and McDermott et al., 2015). We suggest that CH_4 in the hot-spring fluids studied here originates not within actively-circulating fluids, but instead formed elsewhere and was entrained into the fluids prior to venting, as was suggested for Von Damm by McDermott et al. (2015).

Concentrations of CH_4 for the four hydrothermal fields investigated in this study range from 0.86 to 2.81 mM (Fig. 6B). Millimolar concentrations are typical of many ultramafic-hosted mid-ocean ridge hydrothermal fields, whereas basalt-hosted fields tend to have lower CH_4 contents (~0.05 to 1 mM; McCollom and Seewald, 2007; Keir, 2010). While CH_4 concentrations vary less than four-fold (from 0.9 to 2.8 mM), the studied fluids show a wide range of pH (3.3 to 10.2), $\sum CO_2$ (<0.2 to 110 mM) and H_2 (0.03 to 18.2 mM) concentrations (Table 2).

The concentration of dissolved H_2 is high and varies from 10.4 to 18.2 mM in endmember fluids from the Rainbow, Von Damm, and Lost City fields, whereas fluids from Lucky Strike have concentrations of H_2 that are approximately three orders of magnitude lower (34–63 µM, Fig. 6A). At Rainbow, Von Damm, and Lost City, serpentinization of ultramafic rock in subsurface reaction zones (and concomitant H_2 production) is thought to be a major control on fluid compositions (Kelley et al., 2001; Charlou et al., 2002; McDermott et al., 2015). In contrast, the Lucky Strike field is hosted in mafic rocks, and vent fluids there encounter much more oxidizing conditions (Charlou et al., 2000; Pester et al., 2012). At Lucky Strike, synthesis of CH_4 within the low-H_2 endmember fluids is thermodynamically unfavorable at *in situ* temperatures (270–292 °C; Table 2 and Fig. 1B), and becomes even more unfavorable with increasing temperature (Fig. 1A). In all other vent fluids studied here, a thermodynamic drive for CH_4 synthesis is present at varying magnitudes (Fig. 6D). Thus, apparent decoupling of CH_4 concentrations from thermodynamic drives dictated by vent fluid chemistry ($\sum CO_2$, H_2 and pH) and temperature suggests that CH_4 is generated independently at depth, and that conditions under which CH_4 forms are different from those observed at venting.

Endmember fluids from Rainbow, Von Damm, and Lucky Strike contain 2 to 50 times as much total carbon as is in bottom seawater (~2.2 mM; McDermott et al., 2015; Reeves et al., 2014), such that $\sum CO_2$ in recharging seawater cannot be the sole source of carbon to venting fluids. The highly-alkaline Lost City fluid (pH 10.2) contains very low amounts of $\sum CO_2$ (<0.18 mmol/kg), the majority of which is likely derived from seawater entrainment during sample collection (Reeves et al., 2014). At Lost City, Proskurowski et al. (2008) suggested that CH_4 forms via $\sum CO_2$ reduction within the circulating fluids. This model is problematic because it requires the addition of mantle-derived CO_2 to the fluid and immediate reduction to CH_4 thereafter before $\sum CO_2$ can be removed by carbonate precipitation. While sluggish kinetics characterize reduction of $\sum CO_2$ to CH_4, carbonate precipitation proceeds much more rapidly at temperatures experienced by the circulating fluids (Kelemen et al., 2011; Grozeva et al., 2017). (We note that it is possible to generate CH_4 directly from carbonate minerals, for example via hydrogenation reactions, as demonstrated by Giardini et al. (1968) and Yoshida et al. (1999), among others. However, those experiments were carried out with metal (e.g., Co, Ni and Cu) carbonate, the reactions involved are remarkably slow below 400 °C, and their relevance to natural systems is doubtful.) This difference in kinetics means that barring some unidentified catalytic process, $\sum CO_2$ reduction within the circulating hydrothermal fluid—and particularly at the low temperatures postulated by Proskurowski et al. (2006)—does not explain the CH_4 venting from Lost City because $\sum CO_2$ reduction cannot occur in the absence of there being any $\sum CO_2$ to reduce.

The clumped isotopologue temperature obtained for the Lost City methane (270^{+104}_{-68} °C) overlaps with or is slightly higher than temperature estimates from heat balance considerations, $\delta^{18}O$ values, and alkane-alkene and mineral-fluid equilibria that all suggest that fluids beneath Lost City experienced temperatures as high as 200 to 250 °C (Allen and Seyfried, 2004; Foustoukos et al., 2008; Reeves et al., 2012; Seyfried et al., 2015). Agreement between temperatures derived from $\Delta^{13}CH_3D$ and these other geothermometers could be a matter of circumstance (e.g., if all have similar closure temperatures), however, and does not necessarily mean that CH_4 formed and equilibrated its C–H bonds within the same fluids that the other equilibria are recording. Instead, CH_4 may have formed and attained isotopologue equilibrium independently of (outside) the circulating fluids, and later was entrained into them prior to venting. For example, a component of the hydrothermal fluid may have percolated very deeply via meandering flow paths (Titarenko and McCaig, 2016), taking significantly longer to reach seafloor vents and seeing higher temperatures than the remainder of the vent fluid (Hasenclever et al., 2014). If this nearly-stagnant "long-path" fluid was also CH_4-laden, mixing of a minute proportion of this fluid with a CH_4-poor "short-path" hydrothermal fluid could be the source of the up to millimolar quantities of CH_4 emanating from sediment-free seafloor vent systems.

Fluid inclusions record the widespread occurrence and composition of such a CH_4-rich aqueous fluid within the sub-oceanic ridge lithosphere. Kelley (1996; 1997) and Kelley and Früh-Green (1999) documented several types of volatile-rich inclusions hosted in plutonic rocks (gabbros) recovered from the slow-spreading Southwest Indian and Mid-Atlantic Ridges by several Ocean Drilling Program (ODP) expeditions. They noted a common type of inclusion occurring along healed microcracks in plagioclase grains (i.e., secondary inclusions) that contained up to 47 mole percent CH_4 (with balance of H_2O), as well as possibly graphite and H_2. Temperatures indicated by CO_2–CH_4 carbon isotope geothermometry (300–600 °C) and homogenization temperatures of the Southwest Indian Ridge fluid inclusions (350–370 °C, corresponding to entrapment at *in situ* temperatures of ca. 400 °C) (Kelley and Früh-Green, 1999) were interpreted to indicate formation of CH_4 during re-speciation of trapped magmatic volatiles from CO_2 to CH_4 (± graphite) as the melt-derived host rocks cooled to below 400 °C at redox conditions near the FMQ buffer (fayalite-magnetite-quartz, Fig. 2A; Kelley, 1996).

The $\delta^{13}C$ values of CH_4 in vent fluids from unsedimented fields (−24 to −6‰, Supplementary Fig. 2A; Keir, 2010; McCollom and Seewald, 2007) are generally consistent with those determined by analyses of CH_4 in the inclusions. Values for inclusions can be somewhat lower (−34 to −20‰; Kelley and Früh-Green, 1999), probably due to contamination by relatively ^{13}C-depleted thermogenic CH_4 released from background carbon sources during heating of samples to decrepitate the inclusions. In both vent fluids and inclusions, CH_4 is generally more ^{13}C-depleted than mantle-derived CO_2 (−5‰; references in Fig. 1A caption).[5] This presents a mass-balance issue because a ^{13}C-enriched component is apparently missing. Consistent with this, $CH_4/^3He$ ratios in vent fluids (see Keir, 2010) indicate less-than-quantitative conversion (~0.2% to 50%) of mantle carbon to CH_4 (assuming mantle $C/^3He$ is 1×10^9, Marty and Tolstikhin, 1998). Precipitation of graphite from a CH_4-rich fluid entrapped in plutonic rocks may explain both the missing carbon (McDermott et al., 2015) and the observed $\delta^{13}C$ values (Luque et al., 2012). Graphite precipitation in trapped fluids, suggested by Kelley (1996) and others, is consistent with thermodynamic calculations that show that graphite can co-exist with CH_4 at ca. 400 °C under H_2O-poor conditions and redox situated close to FMQ (French, 1966; Eugster and Skippen, 1967; Ohmoto and Kerrick, 1977; Holloway, 1984; Früh-Green et al., 2004).

Concentrations of CH_4 in the fluid inclusions (up to 47 mole percent) from the Southwest Indian Ridge and from other slow-spreading areas can be several orders of magnitude greater than those observed in corresponding vent fluids (on the order of 1 mmol/kg, or 0.002 mole percent) (Kelley, 1996; Kelley, 1997). Mass-balance analysis indicates that extraction of CH_4-rich fluids trapped in plutonic rocks can explain the observed CH_4 concentrations at sediment-free mid-ocean ridge hydrothermal fields. Mixing curves plotted in Fig. 7 show that addition of less than 0.1% of a CH_4-rich fluid of similar composition to those indicated by the inclusions (10 mole percent; *Fluid 2* in the figure) to a CH_4-poor circulating hydrothermal fluid (*Fluid 1*) is sufficient to match even the highest CH_4 concentrations seen in vent fluids. Assuming carbon contents ranging from 30 to 300 ppm in the gabbro (Kelley and Früh-Green, 1999), water-to-rock ratios between 0.8 and 8 can explain CH_4 concentrations of up to 3 mmol/kg in vent fluids assuming all carbon in gabbro existed as leachable CH_4. These water-to-rock ratios are consistent with constraints from Li, Rb, and Sr, which indicate ratios <<10 in many mid-ocean ridge hydrothermal systems (Von Damm et al., 1985; Berndt et al., 1989); values of 0.4 to 6 and 2 to 4, respectively, were calculated at Von Damm and Lost City for instance (Foustoukos et al., 2008; McDermott, 2015).

The above discussion shows that production of CH_4 within actively-circulating hydrothermal fluids is unlikely to account for concentrations and isotopic signatures observed at several studied vent fields. Instead, our data are

[5] Supplementary Fig. 2B shows that $\delta^{13}C$ values of CH_4 and CO_2 in seafloor vent fluids are not correlated. This provides further evidence that CH_4 does not derive from CO_2 in actively-circulating fluids.

compatible with the idea that CH_4-rich fluids trapped in plutonic rocks are liberated during convective hydrothermal circulation, and that the fluids that the CH_4-rich inclusions represent could be the major source of CH_4 in hot-spring fluids at sediment-free oceanic spreading centers. We speculate that these inclusions may have formed during reactions between magmatic volatiles and mafic minerals during incipient percolation of seawater into melt-derived rocks. Available data do not allow us to determine whether direct leaching of the fluid inclusions themselves is the source of CH_4 to endmember hot-spring fluids, or whether both the vent fluid CH_4 and the fluids cached in the inclusions have a common source (i.e., the inclusions simply record a prior passage through plutonic rocks, via small fractures and/or mineral interstices, of the same slowly-moving CH_4-laden parent fluid as those that contribute the CH_4 venting today); both are possible and indeed likely.

While only slow-spreading environments were investigated in this study, the same origin of CH_4 might apply at sites on fast-spreading ridges such as the East Pacific Rise, particularly given the similar $\delta^{13}C$ values for CH_4 (Welhan and Craig, 1983). Concentrations of CH_4 (and C_{2+}) in vent fluids there tend to be lower relative to sites on slow-spreading ridges (Welhan, 1988b; Keir, 2010). Differences in axial structure and tectonism may account for this pattern. At magma-poor slow-spreading ridges, extension is accommodated primarily by detachment faulting, as opposed to magmatic emplacement of new crust that characterizes fast-spreading ridges (Buck et al., 2005; Dunn, 2007). Low-angle, large-offset, and long-lived (>1 Myr) normal faults near vent fields at slow-spreading ridges allow for fluid penetration deep into plutonic rocks of layer 3, enabling access to fresh gabbroic material and/or inclusions to be leached (Kelley, 1996; Schroeder et al., 2002; Schlindwein and Schmid, 2016). In contrast, in fast spreading environments such as the East Pacific Rise, shallow melt lenses at 1 to 2 km below seafloor may limit the depth of circulation (e.g., Hasenclever et al., 2014, and references in Alt, 1995). Lucky Strike, though hosted in mafic rock, is characterized by an unusually deep reaction zone (>3 km) and axial magma chamber, as well as deeply penetrating fault reflectors (e.g. Pester et al., 2012, Escartin et al., 2015 and references therein); thus, circulation there could lead to increased leaching of CH_4 relative to mafic-hosted systems in faster-spreading settings. Efforts to define CH_4 origin will benefit from rigorous interrogation of factors governing fluid flow and chemical kinetics in hydrothermally-influenced settings.

5. CONCLUSIONS

Measured abundances of methane isotopologues in fluids venting from diverse unsedimented mid-ocean ridge hydrothermal systems are highly uniform, and yield last equilibration temperatures of ca. 300 °C for the C–H bond. Taken in combination with geochemical and geologic observations and reaction rates determined in experiments, the $\Delta^{13}CH_3D$ data establish that abiotic reduction of $\sum CO_2$ (via e.g., FTT synthesis) at low temperatures (<200 °C) is unlikely to be a significant source of methane over timescales characterizing convective hydrothermal circulation at oceanic spreading centers. Apparent decoupling between methane isotopologue abundances and vent fluid chemistry points to a deep origin of CH_4 that is disconnected from active hydrothermal circulation.

We believe that the available data are best explained by a model where fluids rich in CH_4 (up to tens of mole percent) form within plutonic rocks during re-speciation of magmatic carbon trapped in fluid inclusions or interstitial spaces between mineral grains at temperatures at above 300 °C and under low water-to-rock ratios, and are later leached into circulating hydrothermal fluids. Vent fluids with millimolar quantities of CH_4 therefore represent mixing of a minute amount of a CH_4-rich fluid with a large volume of an actively-circulating, CH_4-poor fluid. Proportions of mixing may be determined by the relative access that circulating fluids have to magmatic volatile-bearing rocks of the plutonic foundation. Such a model could explain apparent relationships of CH_4 concentration in vent fluids to tectonic setting and host rock lithology. It also explains the apparent lack of correlation between

CH_4 concentrations and thermodynamic drive for CH_4 synthesis calculated for chemical compositions and temperatures of the venting fluids.

The new data also place constraints on the closure temperature of hydrogen exchange between methane and water. The observation of sluggish or indiscernible exchange of H among methane isotopologues below ca. 300 °C on timescales of ~10^2 years is relevant not only to the application of clumped isotope measurements as a novel geothermometer, but also provides information about the stability of the C–H bond in hydrocarbons in nature. Given the increasing appreciation of hydrocarbon-water-mineral interactions in economically important settings (Seewald, 2003), insights of this nature may find utility in studies of the origin and composition of aqueous and organic fluids in the Earth's subsurface.

6. ACKNOWLEDGMENTS

We thank Frieder Klein, Wolfgang Bach, Grant Garven, and Meg Tivey for insightful discussions regarding the petrology and plumbing of hydrothermal systems. Thoughtful reviews by Dionysis Foustoukos, Shinsuke Kawagucci, and Daniel Stolper are greatly appreciated. Financial support from the U.S. National Science Foundation (NSF awards EAR-1250394 to S.O., and OCE-1061863 and OCE-0549829 to J.S.S.), the National Aeronautics and Space Administration (NASA) (NNX-327 09AB75G to J.S.S., and the NASA Astrobiology Institute "Rock-Powered Life" project under cooperative agreement NNA15BB02A to S.O.), the Alfred P. Sloan Foundation via the Deep Carbon Observatory (to S.O. and J.S.S.), the U.S. Department of Defense (DoD) through a National Defense Science & Engineering Graduate (NDSEG) Fellowship (to D.T.W.), a Shell-MIT Energy Initiative Fellowship, and the Kerr-McGee Professorship at MIT (to S.O.) is gratefully acknowledged.

Supplementary Material is included with this submission.

7. REFERENCES

Allen D. E. and Seyfried W. (2004) Serpentinization and heat generation: constraints from Lost City and Rainbow hydrothermal systems. *Geochimica et Cosmochimica Acta* **68**, 1347–1354.

Alt J. C. (1995) Subseafloor processes in mid-ocean ridge hydrothermal systems. In *Seafloor Hydrothermal Systems: Physical, Chemical, Biological, and Geological Interactions* Wiley-Blackwell. pp. 85–114.

Bacsik Z., Lopes J. N. C., Gomes M. F. C., Jancsó G., Mink J. and Pádua A. A. H. (2002) Solubility isotope effects in aqueous solutions of methane. *The Journal of Chemical Physics* **116**, 10816–10824.

Bardo R. D. and Wolfsberg M. (1976) A theoretical calculation of the equilibrium constant for the isotopic exchange reaction between water and hydrogen deuteride. *The Journal of Physical Chemistry* **80**, 1068–1071.

Berndt M. E., Seyfried W. E. and Janecky D. R. (1989) Plagioclase and epidote buffering of cation ratios in mid-ocean ridge hydrothermal fluids: Experimental results in and near the supercritical region. *Geochimica et Cosmochimica Acta* **53**, 2283–2300.

Blank J. G., Delaney J. R. and Des Marais D. J. (1993) The concentration and isotopic composition of carbon in basaltic glasses from the Juan de Fuca Ridge, Pacific Ocean. *Geochimica et Cosmochimica Acta* **57**, 875–887.

Bradley A. S. and Summons R. E. (2010) Multiple origins of methane at the Lost City Hydrothermal Field. *Earth and Planetary Science Letters* **297**, 34–41.

Brazelton W. J., Schrenk M. O., Kelley D. S. and Baross J. A. (2006) Methane-and sulfur-metabolizing microbial communities dominate the Lost City hydrothermal field ecosystem. *Applied and Environmental Microbiology* **72**, 6257–6270.

Buck W. R., Lavier L. L. and Poliakov A. N. (2005) Modes of faulting at mid-ocean ridges. *Nature* **434**, 719–723.

Campbell B. J., Li C., Sessions A. L. and Valentine D. L. (2009) Hydrogen isotopic fractionation in lipid biosynthesis by H_2-consuming *Desulfobacterium autotrophicum*. *Geochimica et Cosmochimica Acta* **73**, 2744–2757.

Cannat M., Fontaine F. and Escartin J. (2010) Serpentinization and associated hydrogen and methane fluxes at slow spreading ridges. *Diversity of hydrothermal systems on slow spreading ocean ridges*, 241–264.

Cerrai E., Marchetti C., Renzoni R., Roseo L., Silvestri M. and Villani S. (1954) A Thermal Method for Concentrating Heavy Water. Nuclear Engineering, Part I. In *Chem. Eng. Progr. Symposium Ser.* Laboratori CISE, Milan, Italy. pp. 271–280.

Charlou J., Donval J., Douville E., Jean-Baptiste P., Radford-Knoery J., Fouquet Y., Dapoigny A. and Stievenard M. (2000) Compared geochemical signatures and the evolution of Menez Gwen (37°50' N) and Lucky Strike (37°17'N) hydrothermal fluids, south of the Azores Triple Junction on the Mid-Atlantic Ridge. *Chemical Geology* **171**, 49–75.

Charlou J., Donval J., Fouquet Y., Jean-Baptiste P. and Holm N. (2002) Geochemistry of high H_2 and CH_4 vent fluids issuing from ultramafic rocks at the Rainbow hydrothermal field (36°14'N, MAR). *Chemical Geology* **191**, 345–359.

Charlou J. L., Donval J. P., Konn C., Ondréas H., Fouquet Y., Jean-Baptiste P. and Fourré E. (2010) High production and fluxes of H_2 and CH_4 and evidence of abiotic hydrocarbon synthesis by serpentinization in ultramafic-hosted hydrothermal systems on the Mid-Atlantic Ridge. *Diversity of hydrothermal systems on slow spreading ocean ridges*, 265–296.

Clayton C. (2003) Hydrogen isotope systematics of thermally generated natural gas. *Int. Meet. Org. Geochem., 21st, Kraków, Poland, Book Abstr. Part I*, 51–52.

Clog M., Aubaud C., Cartigny P. and Dosso L. (2013) The hydrogen isotopic composition and water content of southern Pacific MORB: A reassessment of the D/H ratio of the depleted mantle reservoir. *Earth and Planetary Science Letters* **381**, 156–165.

Crist R. H. and Dalin G. A. (1933) Exchange reactions of protium and deuterium. *The Journal of Chemical Physics* **1**, 677–677.

Cruse A. M. and Seewald J. S. (2006) Geochemistry of low-molecular weight hydrocarbons in hydrothermal fluids from Middle Valley, northern Juan de Fuca Ridge. *Geochimica et Cosmochimica Acta* **70**, 2073–2092.

Dick J. M. (2008) Calculation of the relative metastabilities of proteins using the CHNOSZ software package. *Geochemical Transactions* **9**, 10.

Douglas P., Stolper D., Smith D., Anthony K. W., Paull C., Dallimore S., Wik M., Crill P., Winterdahl M., Eiler J. and Sessions A. (2016) Diverse origins of Arctic and Subarctic methane point source emissions identified with multiply-substituted isotopologues. *Geochimica et Cosmochimica Acta* **188**, 163–188.

Douglas P. M. J., Stolper D. A., Eiler J. M., Sessions A. L., Lawson M., Shuai Y., Bishop A., Podlaha O. G., Ferreira A. A., Neto E. V. S., Niemann M., Steen A. S., Huang L., Chimiak L., Valentine D. L., Fiebig J., Luhmann A. J., Seyfried W. E., Etiope G., Schoell M., Inskeep W. P., Moran J. J. and Kitchen N. (2017) Methane clumped isotopes: Progress and potential for a new isotopic tracer. *Organic Geochemistry* **113**, 262–282.

Dunn R. (2007) Crust and lithospheric structure—seismic structure of mid-ocean ridges. In *Treatise in Geophysics* (ed. G. Schubert). Treatise In Geophysics. Elsevier. pp. 419–443.

Eiler J. M. (2007) “Clumped-isotope” geochemistry—The study of naturally-occurring, multiply-substituted isotopologues. *Earth and Planetary Science Letters* **262**, 309–327.

Escartin J., Barreyre T., Cannat M., Garcia R., Gracias N., Deschamps A., Salocchi A., Sarradin P.-M. and Ballu V. (2015) Hydrothermal activity along the slow-spreading Lucky Strike ridge segment (Mid-Atlantic Ridge): Distribution, heatflux, and geological controls. *Earth and Planetary Science Letters* **431**, 173–185.

Eugster H. and Skippen G. (1967) Igneous and metamorphic reactions involving gas equilibria. In *Researches in geochemistry* (ed. P. Abelson). Wiley New York, NY. pp. 492–520.

Fisher A. T. (2003) Geophysical Constraints on Hydrothermal Circulation: Observations and Models. In *Energy and mass transfer in marine hydrothermal systems* (eds. P. Halbach, V. Tunnicliffe, and J. R. Hein). Dahlem workshop reports. Dahlem University Press. pp. 29–52.

Foustoukos D. I., Savov I. P. and Janecky D. R. (2008) Chemical and isotopic constraints on water/rock interactions at the Lost City hydrothermal field, 30°N Mid-Atlantic Ridge. *Geochimica et Cosmochimica Acta* **72**, 5457–5474.

French B. M. (1966) Some geological implications of equilibrium between graphite and a C-H-O gas phase at high temperatures and pressures. *Reviews of Geophysics* **4**, 223.

Früh-Green G. L., Connolly J. A., Plas A., Kelley D. S. and Grobéty B. (2004) Serpentinization of oceanic peridotites: implications for geochemical cycles and biological activity. *The Subseafloor Biosphere at Mid-Ocean Ridges*, 119–136.

Gould A. J., Bleakney W. and Taylor H. S. (1934) The Inter-Relations of Hydrogen and Deuterium Molecules. *The Journal of Chemical Physics* **2**, 362–373.

Grozeva N. G., Klein F., Seewald J. S. and Sylva S. P. (2017) Experimental study of carbonate formation in oceanic peridotite. *Geochimica et Cosmochimica Acta* **199**, 264–286.

Hall N. F., Bowden E. and Jones T. (1934) Exchange reactions of hydrogen atoms. *Journal of the American Chemical Society* **56**, 750–750.

Hasenclever J., Theissen-Krah S., Rüpke L. H., Morgan J. P., Iyer K., Petersen S. and Devey C. W. (2014) Hybrid shallow on-axis and deep off-axis hydrothermal circulation at fast-spreading ridges. *Nature* **508**, 508–512.

Hoering T. (1984) Thermal reactions of kerogen with added water, heavy water and pure organic substances. *Organic Geochemistry* **5**, 267–278.

Holloway J. R. (1984) Graphite-CH_4-H_2O-CO_2 equilibria at low-grade metamorphic conditions. *Geology* **12**, 455–458.

Horibe Y. and Craig H. (1995) D/H fractionation in the system methane-hydrogen-water. *Geochimica et Cosmochimica Acta* **59**, 5209–5217.

Horita J. and Wesolowski D. J. (1994) Liquid-vapor fractionation of oxygen and hydrogen isotopes of water from the freezing to the critical temperature. *Geochimica et Cosmochimica Acta* **58**, 3425–3437.

Hulston J. (1977) Isotope work applied to geothermal systems at the Institute of Nuclear Sciences, New Zealand. *Geothermics* **5**, 89–96.

Inagaki F., Hinrichs K.-U., Kubo Y., Bowles M. W., Heuer V. B., Hong W.-L., Hoshino T., Ijiri A., Imachi H., Ito M., Kaneko M., Lever M. A., Lin Y.-S., Methe B. A., Morita S., Morono Y., Tanikawa W., Bihan M., Bowden S. A., Elvert M., Glombitza C., Gross D., Harrington G. J., Hori T., Li K., Limmer D., Liu C.-H., Murayama M., Ohkouchi N., Ono S., Park Y.-S., Phillips S. C., Prieto-Mollar X., Purkey M., Riedinger N., Sanada Y., Sauvage J., Snyder G., Susilawati R., Takano Y., Tasumi E., Terada T., Tomaru H., Trembath-Reichert E., Wang D. T. and Yamada Y. (2015) Exploring deep microbial life in coal-bearing sediment down to ~2.5 km below the ocean floor. *Science* **349**, 420–424.

Javoy M., Pineau F. and Delorme H. (1986) Carbon and nitrogen isotopes in the mantle. *Chemical geology* **57**, 41–62.

Johnson J. W., Oelkers E. H. and Helgeson H. C. (1992) SUPCRT92: A software package for calculating the standard molal thermodynamic properties of minerals, gases, aqueous species, and reactions from 1 to 5000 bar and 0 to 1000 °C. *Computers & Geosciences* **18**, 899–947.

Kadko D. (1996) Radioisotopic studies of submarine hydrothermal vents. *Reviews of Geophysics* **34**, 349–366.

Kawagucci S., Toki T., Ishibashi J., Takai K., Ito M., Oomori T. and Gamo T. (2010) Isotopic variation of molecular hydrogen in 20°–375°C hydrothermal fluids as detected by a new analytical method. *Journal of Geophysical Research: Biogeosciences* **115**, G03021.

Kawagucci S., Ueno Y., Takai K., Toki T., Ito M., Inoue K., Makabe A., Yoshida N., Muramatsu Y., Takahata N., Sano Y., Narita T., Teranishi G., Obata H., Nakagawa S., Nunoura T. and Gamo T. (2013) Geochemical origin of hydrothermal fluid methane in sediment-associated fields and its relevance to the geographical distribution of whole hydrothermal circulation. *Chemical Geology* **339**, 213–225.

Keir R. (2010) A note on the fluxes of abiogenic methane and hydrogen from mid-ocean ridges. *Geophysical Research Letters* **37**.

Kelemen P. B., Matter J., Streit E. E., Rudge J. F., Curry W. B. and Blusztajn J. (2011) Rates and mechanisms of mineral carbonation in peridotite: natural processes and recipes for enhanced, in situ CO_2 capture and storage. *Annual Review of Earth and Planetary Sciences* **39**, 545–576.

Kelley D. S. (1997) Fluid evolution in slow-spreading environments. In *Proceedings of the Ocean Drilling Program. Scientific Results* Ocean Drilling Program. pp. 399–415.

Kelley D. S. (1996) Methane-rich fluids in the oceanic crust. *Journal of Geophysical Research: Solid Earth* **101**, 2943–2962.

Kelley D. S. and Früh-Green G. L. (1999) Abiogenic methane in deep-seated mid-ocean ridge environments: Insights from stable isotope analyses. *Journal of Geophysical Research: Solid Earth* **104**, 10439–10460.

Kelley D. S., Karson J. A., Blackman D. K., Früh-Green G. L., Butterfield D. A., Lilley M. D., Olson E. J., Schrenk M. O., Roe K. K., Lebon G. T., Rivizzigno P. and the AT3-60 Shipboard Party (2001) An off-axis hydrothermal vent field near the Mid-Atlantic Ridge at 30° N. *Nature* **412**, 145–149.

Klein F., Bach W., Jöns N., McCollom T., Moskowitz B. and Berquó T. (2009) Iron partitioning and hydrogen generation during serpentinization of abyssal peridotites from 15° N on the Mid-Atlantic Ridge. *Geochimica et Cosmochimica Acta* **73**, 6868–6893.

Klein F., Bach W. and McCollom T. M. (2013) Compositional controls on hydrogen generation during serpentinization of ultramafic rocks. *Lithos* **178**, 55–69.

Koepp M. (1978) D/H isotope exchange reaction between petroleum and water: a contributory determinant for D/H-isotope ratios in crude oils. In *The Fourth International Conference, Geochronology, Cosmochronology, Isotope Geology USGS Open-File Report 78-701* pp. 221–222.

Lécluse C. and Robert F. (1994) Hydrogen isotope exchange reaction rates: Origin of water in the inner solar system. *Geochimica et Cosmochimica Acta* **58**, 2927–2939.

Lewan M. (1997) Experiments on the role of water in petroleum formation. *Geochimica et Cosmochimica Acta* **61**, 3691–3723.

Lilley M., Butterfield D., Olson E., Lupton J., Macko S. and McDuff R. (1993) Anomalous CH_4 and NH_4^+ concentrations at an unsedimented mid-ocean-ridge hydrothermal system. *Nature* **364**, 45–47.

Lin L.-H., Slater G. F., Lollar B. S., Lacrampe-Couloume G. and Onstott T. (2005) The yield and isotopic composition of radiolytic H_2, a potential energy source for the deep subsurface biosphere. *Geochimica et Cosmochimica Acta* **69**, 893–903.

Lis G. P., Schimmelmann A. and Mastalerz M. (2006) D/H ratios and hydrogen exchangeability of type-II kerogens with increasing thermal maturity. *Organic Geochemistry* **37**, 342–353.

Luque F. J., Crespo-Feo E., Barrenechea J. F. and Ortega L. (2012) Carbon isotopes of graphite: Implications on fluid history. *Geoscience Frontiers* **3**, 197–207.

Lyon G. and Hulston J. (1984) Carbon and hydrogen isotopic compositions of New Zealand geothermal gases. *Geochimica et Cosmochimica Acta* **48**, 1161–1171.

Marty B. and Tolstikhin I. N. (1998) CO_2 fluxes from mid-ocean ridges, arcs and plumes. *Chemical Geology* **145**, 233–248.

McCollom T. M. (2016) Abiotic methane formation during experimental serpentinization of olivine. *Proceedings of the National Academy of Sciences of the United States of America* **113**, 13965–13970.

McCollom T. M. and Seewald J. S. (2001) A reassessment of the potential for reduction of dissolved CO_2 to hydrocarbons during serpentinization of olivine. *Geochimica et Cosmochimica Acta* **65**, 3769–3778.

McCollom T. M. and Seewald J. S. (2007) Abiotic synthesis of organic compounds in deep-sea hydrothermal environments. *Chemical Reviews* **107**, 382–401.

McCollom T. M. and Seewald J. S. (2003) Experimental constraints on the hydrothermal reactivity of organic acids and acid anions: I. Formic acid and formate. *Geochimica et Cosmochimica Acta* **67**, 3625–3644.

McDermott J. M. (2015) Geochemistry of deep-sea hydrothermal vent fluids from the Mid-Cayman Rise, Caribbean Sea. Thesis, Massachusetts Institute of Technology and Woods Hole Oceanographic Institution.

McDermott J. M., Seewald J. S., German C. R. and Sylva S. P. (2015) Pathways for abiotic organic synthesis at submarine hydrothermal fields. *Proceedings of the National Academy of Sciences of the United States of America* **112**, 7668–7672.

Muccitelli J. and Wen W.-Y. (1978) Solubilities of hydrogen and deuterium gases in water and their isotope fractionation factor. *Journal of Solution Chemistry* **7**, 257–267.

Ohmoto H. and Kerrick D. M. (1977) Devolatilization equilibria in graphitic systems. *American Journal of Science* **277**, 1013–1044.

Ono S., Wang D. T., Gruen D. S., Sherwood Lollar B., Zahniser M., McManus B. J. and Nelson D. D. (2014) Measurement of a doubly-substituted methane isotopologue, $^{13}CH_3D$, by tunable infrared laser direct absorption spectroscopy. *Analytical Chemistry* **86**, 6487–6494.

Pester N. J., Reeves E. P., Rough M. E., Ding K., Seewald J. S. and Seyfried W. E. (2012) Subseafloor phase equilibria in high-temperature hydrothermal fluids of the Lucky Strike Seamount (Mid-Atlantic Ridge, 37°17′N). *Geochimica et Cosmochimica Acta* **90**, 303–322.

Proskurowski G. (2010) Abiogenic hydrocarbon production at the geosphere-biosphere interface via serpentinization reactions. In *Handbook of Hydrocarbon and Lipid Microbiology* (ed. K. N. Timmis). Springer. pp. 215–231.

Proskurowski G., Lilley M. D., Kelley D. S. and Olson E. J. (2006) Low temperature volatile production at the Lost City Hydrothermal Field, evidence from a hydrogen stable isotope geothermometer. *Chemical Geology* **229**, 331–343.

Proskurowski G., Lilley M. D., Seewald J. S., Früh-Green G. L., Olson E. J., Lupton J. E., Sylva S. P. and Kelley D. S. (2008) Abiogenic hydrocarbon production at Lost City hydrothermal field. *Science* **319**, 604–607.

Reeves E. (2010) Laboratory and field-based investigations of subsurface geochemical processes in seafloor hydrothermal systems. Thesis, Massachusetts Institute of Technology and Woods Hole Oceanographic Institution.

Reeves E. P., McDermott J. M. and Seewald J. S. (2014) The origin of methanethiol in midocean ridge hydrothermal fluids. *Proceedings of the National Academy of Sciences of the United States of America* **111**, 5474–5479.

Reeves E. P., Seewald J. S. and Sylva S. P. (2012) Hydrogen isotope exchange between n-alkanes and water under hydrothermal conditions. *Geochimica et Cosmochimica Acta* **77**, 582–599.

Schimmelmann A., Boudou J.-P., Lewan M. D. and Wintsch R. P. (2001) Experimental controls on D/H and $^{13}C/^{12}C$ ratios of kerogen, bitumen and oil during hydrous pyrolysis. *Organic Geochemistry* **32**, 1009–1018.

Schimmelmann A., Lewan M. D. and Wintsch R. P. (1999) D/H isotope ratios of kerogen, bitumen, oil, and water in hydrous pyrolysis of source rocks containing kerogen types I, II, IIS, and III. *Geochimica et Cosmochimica Acta* **63**, 3751–3766.

Schimmelmann A., Sessions A. L. and Mastalerz M. (2006) Hydrogen isotopic (D/H) composition of organic matter during diagenesis and thermal maturation. *Annual Review of Earth and Planetary Sciences* **34**, 501–533.

Schlindwein V. and Schmid F. (2016) Mid-ocean-ridge seismicity reveals extreme types of ocean lithosphere. *Nature*.

Schroeder T., John B. and Frost B. R. (2002) Geologic implications of seawater circulation through peridotite exposed at slow-spreading mid-ocean ridges. *Geology* **30**, 367–370.

Seewald J. S. (2001) Aqueous geochemistry of low molecular weight hydrocarbons at elevated temperatures and pressures: constraints from mineral buffered laboratory experiments. *Geochimica et Cosmochimica Acta* **65**, 1641–1664.

Seewald J. S. (2003) Organic–inorganic interactions in petroleum-producing sedimentary basins. *Nature* **426**, 327–333.

Seewald J. S., Doherty K. W., Hammar T. R. and Liberatore S. P. (2002) A new gas-tight isobaric sampler for hydrothermal fluids. *Deep Sea Research Part I: Oceanographic Research Papers* **49**, 189–196.

Seewald J. S., Zolotov M. Y. and McCollom T. (2006) Experimental investigation of single carbon compounds under hydrothermal conditions. *Geochimica et Cosmochimica Acta* **70**, 446–460.

Seyfried W. and Ding K. (1995) Phase equilibria in subseafloor hydrothermal systems: A review of the role of redox, temperature, pH and dissolved Cl on the chemistry of hot spring fluids at mid-ocean ridges. In *Seafloor Hydrothermal Systems: Physical, Chemical, Biological, and Geological Interactions* Wiley-Blackwell. pp. 248–272.

Seyfried W., Pester N. J., Tutolo B. M. and Ding K. (2015) The Lost City hydrothermal system: Constraints imposed by vent fluid chemistry and reaction path models on subseafloor heat and mass transfer processes. *Geochimica et Cosmochimica Acta* **163**, 59–79.

Shanks W., Böhlke J. and Seal R. (1995) Stable isotopes in mid-ocean ridge hydrothermal systems: interactions between fluids, minerals, and organisms. In *Seafloor Hydrothermal Systems: Physical, Chemical, Biological, and Geological Interactions, Geophysical Monograph 91* (eds. S. E. Humphris, R. A. Zierenberg, L. S. Mullineaux, and R. E. Thomson). American Geophysical Union, Washington, DC. pp. 194–221.

Sharp J. H., Benner R., Bennett L., Carlson C. A., Fitzwater S. E., Peltzer E. T. and Tupas L. M. (1995) Analyses of dissolved organic carbon in seawater: the JGOFS EqPac methods comparison. *Marine Chemistry* **48**, 91–

108.Shock E. L. (1992) Chapter 5. Chemical environments of submarine hydrothermal systems. *Origins of Life and Evolution of the Biosphere* **22**, 67–107.

Shock E. L. (1990) Geochemical constraints on the origin of organic compounds in hydrothermal systems. *Origins of Life and Evolution of the Biosphere* **20**, 331–367.

Shock E. L. and Helgeson H. C. (1990) Calculation of the thermodynamic and transport properties of aqueous species at high pressures and temperatures: Standard partial molal properties of organic species. *Geochimica et Cosmochimica Acta* **54**, 915–945.

Simoneit B. R., Kawka O. and Brault M. (1988) Origin of gases and condensates in the Guaymas Basin hydrothermal system (Gulf of California). *Chemical Geology* **71**, 169–182.

Sleep N., Meibom A., Fridriksson T., Coleman R. and Bird D. (2004) H_2-rich fluids from serpentinization: geochemical and biotic implications. *Proceedings of the National Academy of Sciences of the United States of America* **101**, 12818–12823.

Smith J., Rigby D., Gould K., Hart G. and Hargraves A. (1985) An isotopic study of hydrocarbon generation processes. *Organic Geochemistry* **8**, 341–347.

Stolper D. A., Lawson M., Davis C. L., Ferreira A. A., Santos Neto E. V., Ellis G. S., Lewan M. D., Martini A. M., Tang Y., Schoell M., Sessions A. L. and Eiler J. M. (2014) Formation temperatures of thermogenic and biogenic methane. *Science* **344**, 1500–1503.

Stolper D., Martini A., Clog M., Douglas P., Shusta S., Valentine D., Sessions A. and Eiler J. (2015) Distinguishing and understanding thermogenic and biogenic sources of methane using multiply substituted isotopologues. *Geochimica et Cosmochimica Acta* **161**, 219–247.

Suess H. (1949) Das Gleichgewicht H_2+ HDO = HD + H_2O und die weiteren Austauschgleichgewichte im System H_2, D_2 und H_2O. *Zeitschrift Naturforschung Teil A* **4**, 328.

Takai K., Nakamura K., Toki T., Tsunogai U., Miyazaki M., Miyazaki J., Hirayama H., Nakagawa S., Nunoura T. and Horikoshi K. (2008) Cell proliferation at 122°C and isotopically heavy CH_4 production by a hyperthermophilic methanogen under high-pressure cultivation. *Proceedings of the National Academy of Sciences of the United States of America* **105**, 10949–10954.

Titarenko S. S. and McCaig A. M. (2016) Modelling the Lost City hydrothermal field: influence of topography and permeability structure. *Geofluids* **16**, 314–328.

Von Damm K. L., Edmond J. M., Grant B., Measures C. I., Walden B. and Weiss R. F. (1985) Chemistry of submarine hydrothermal solutions at 21°N, East Pacific Rise. *Geochimica et Cosmochimica Acta* **49**, 2197–2220.

Wagner W. and Pruß A. (2002) The IAPWS formulation 1995 for the thermodynamic properties of ordinary water substance for general and scientific use. *Journal of Physical and Chemical Reference Data* **31**, 387–535.

Wang D. T. (2017) The geochemistry of methane isotopologues. Ph.D. thesis, Massachusetts Institute of Technology and Woods Hole Oceanographic Institution. doi:10.1575/1912/9052

Wang D. T., Gruen D. S., Lollar B. S., Hinrichs K.-U., Stewart L. C., Holden J. F., Hristov A. N., Pohlman J. W., Morrill P. L., Könneke M., Delwiche K. B., Reeves E. P., Sutcliffe C. N., Ritter D. J., Seewald J. S., McIntosh J. C., Hemond H. F., Kubo M. D., Cardace D., Hoehler T. M. and Ono S. (2015) Nonequilibrium clumped isotope signals in microbial methane. *Science* **348**, 428–431.

Welhan J. A. (1988a) Methane and hydrogen in mid-ocean-ridge basalt glasses: analysis by vacuum crushing. *Canadian Journal of Earth Sciences* **25**, 38–48.

Welhan J. A. (1988b) Origins of methane in hydrothermal systems. *Chemical Geology* **71**, 183–198.

Welhan J. A. and Craig H. (1983) Methane, hydrogen and helium in hydrothermal fluids at 21°N on the East Pacific Rise. In *Hydrothermal Processes at Seafloor Spreading Centers.* Springer. pp. 391–409.

Welhan J. and Lupton J. (1987) Light hydrocarbon gases in Guaymas Basin hydrothermal fluids: thermogenic versus abiogenic origin. *AAPG Bulletin* **71**, 215–223.

Young E. D., Kohl I. E., Lollar B. S., Etiope G., Rumble D., Li S., Haghnegahdar M. A., Schauble E. A., McCain K. A., Foustoukos D. I., Sutclife C., Warr O., Ballentine C. J., Onstott T. C., Hosgormez H., Neubeck A., Marques J. M., Pérez-Rodrıguez I., Rowe A. R., LaRowe D. E., Magnabosco C., Yeung L. Y., Ash J. L. and Bryndzia L. T. (2017) The relative abundances of resolved $^{12}CH_2D_2$ and $^{13}CH_3D$ and mechanisms controlling isotopic bond ordering in abiotic and biotic methane gases. *Geochimica et Cosmochimica Acta* **203**, 235–264.

Yoshida N., Hattori T., Komai E. and Wada T. (1999) Methane formation by metal-catalyzed hydrogenation of solid calcium carbonate. *Catalysis Letters* **58**, 119–122.

8. FIGURES

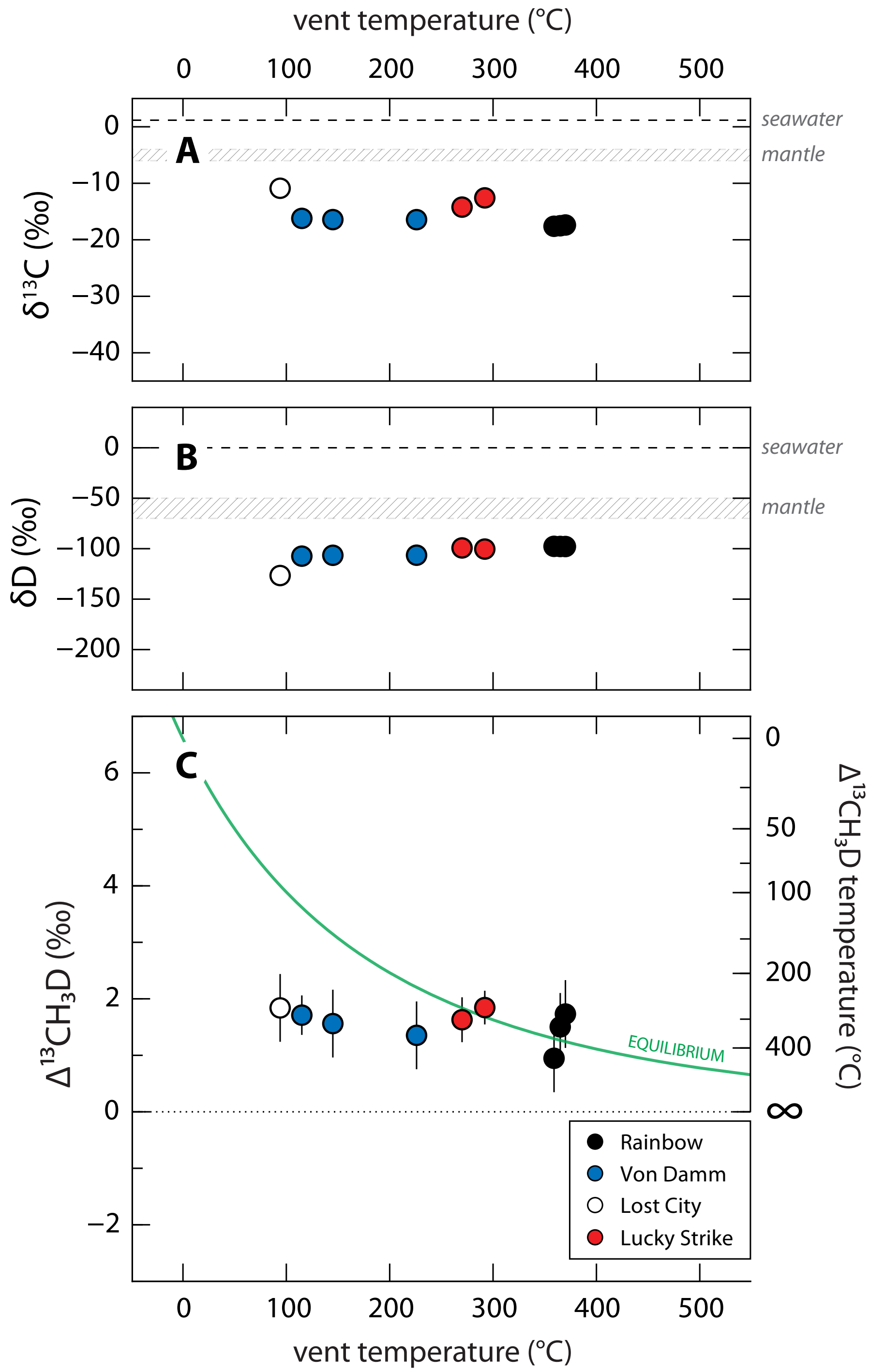

Fig. 1. Comparison of (**A**) $\delta^{13}C$, (**B**) δD, and (**C**) $\Delta^{13}CH_3D$ values of methane across vent sites. Data and error bars (95% confidence interval) are from Table 1. In all panels, data are plotted against measured vent temperature (Table 2). The isotopic compositions of inorganic carbon (A) and hydrogen (B) in seawater and in the mantle are shown (Javoy et al., 1986; Blank et al., 1993; Clog et al., 2013). In (C), the green line represents the clumped isotopologue composition at equilibrium. The $\Delta^{13}CH_3D$ temperature scale corresponds to the calibration from Wang et al. (2015).

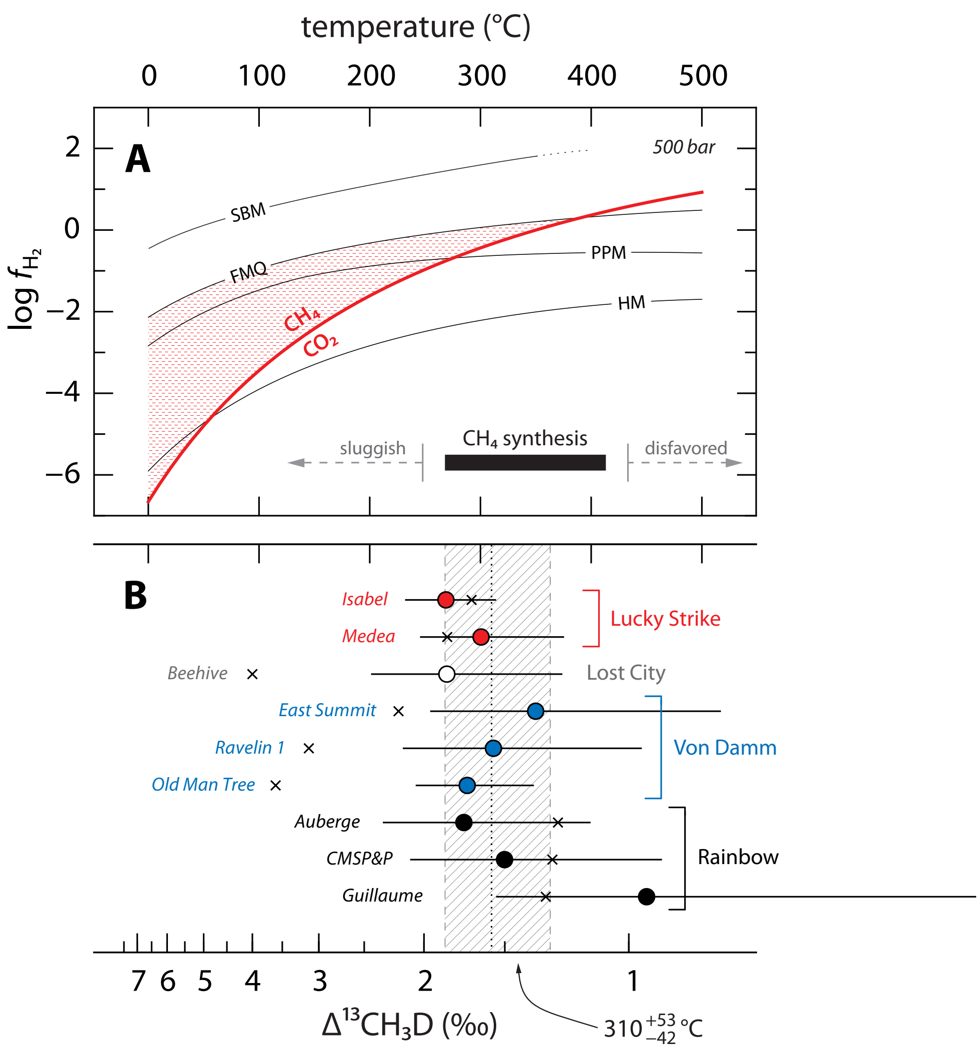

Fig. 2. Constraints on abiotic methane formation and stability from thermodynamics and clumped isotopologue data. (**A**) Plot of fugacity of H_2 as a function of temperature at 500 bar, after Shock (1992). The red line represents the fugacity of H_2 at equilibrium, according to the reaction $CO_2(g) + 4H_2(g) \rightleftharpoons CH_4(g) + 2H_2O(l)$, when the fugacities of CH_4 and CO_2 are equal, and assuming unit activity for $H_2O(l)$. Grey lines represent equilibrium H_2 fugacities buffered by the mineral assemblages hematite-magnetite (HM), pyrite-pyrrhotite-magnetite (PPM), fayalite-magnetite-quartz (FMQ), and serpentine-magnetite-brucite (SBM). The curve for SBM is the is the low-Fe serpentinite from Sleep et al. (2004), and is truncated above 400 °C where serpentinization is unlikely to occur (see Sec. 4.2.3). Red shaded area represents the intersection of regions corresponding to geologically-relevant H_2 fugacity and where CH_4 is thermodynamically stable relative to CO_2. The black bar represents the temperature range over which our interpretation suggests that methane synthesis is both favorable and facile on timescales of relevance to hydrothermal systems. (**B**) Clumped isotopologue temperatures of methane from studied vents (data and error bars from Table 1). Equivalent $\Delta^{13}CH_3D$ values are plotted on the bottom axis, and are derived from the calibration of Wang et al. (2015). The dotted line and gray hatching represent the mean ± 1*s* of the $\Delta^{13}CH_3D$ values across all studied vents (1.57 ± 0.28‰, *n* = 9). The × symbols mark measured vent temperatures (Table 2).

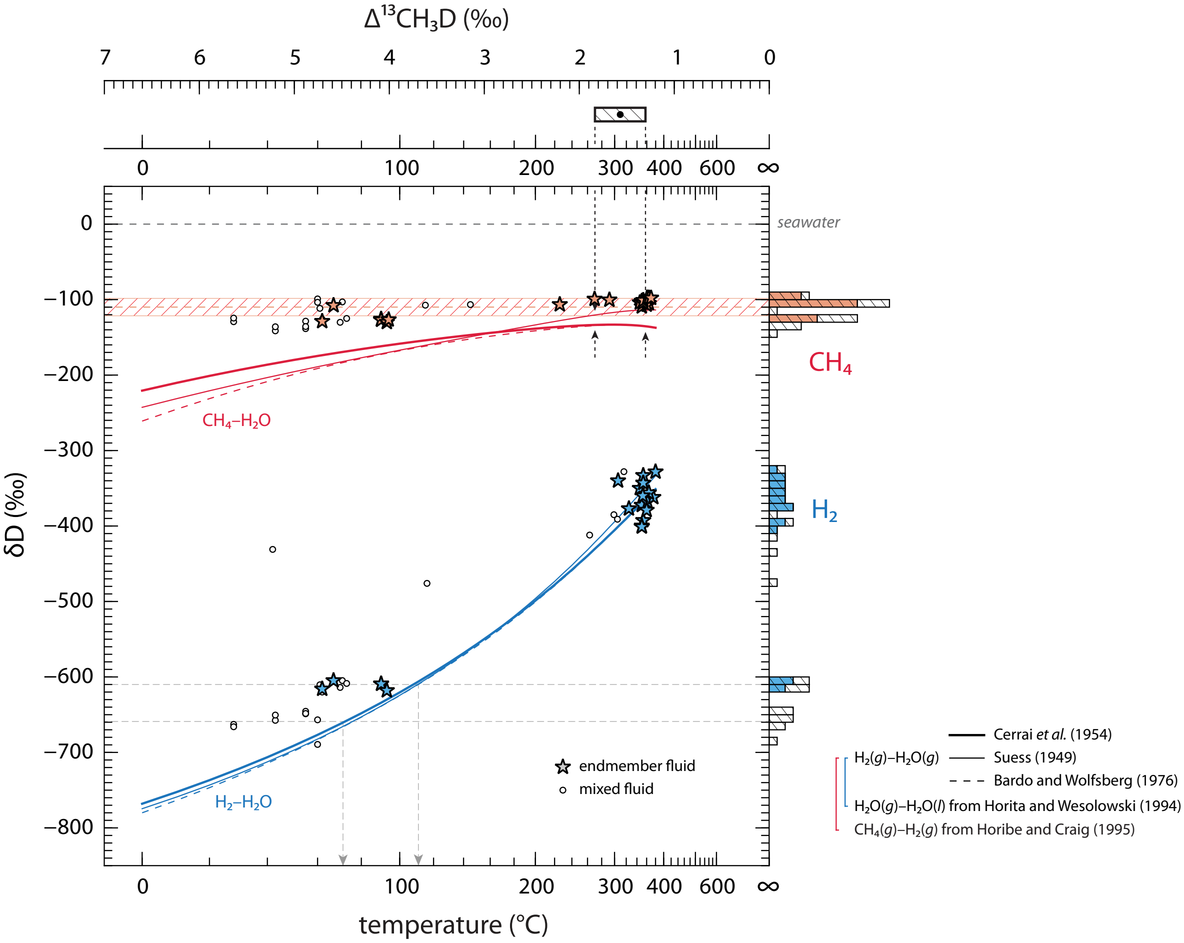

Fig. 3. Hydrogen isotopic composition of CH_4 (red) and H_2 (blue) in seafloor hydrothermal fluids plotted against measured vent temperatures. Data are from unsedimented fields studied by Welhan and Craig (1983), Proskurowski et al. (2006), Kawagucci et al. (2010), Charlou et al. (2010), and us (see Tables 1 and 2), and are tabulated in Supplementary Table 2. Endmember fluids (identified by low Mg contents) are represented by stars, and vent fluids containing a mixture of hydrothermal endmember fluid and seawater are represented by circles. Data from sites exhibiting phase separation (Charlou et al., 2010) or with fluids diffusely effluxing through colonies of deep-sea snails or shrimp (Kawagucci et al., 2010) are excluded from this plot (see note *f* under Supplementary Table 2). Red hatching indicates the average δD of CH_4 in endmember fluids (−110 ± 12‰, 1*s*) in the compiled dataset. Red and blue curves represent the δD values of CH_4 and H_2 (respectively) in D/H equilibrium with seawater-like H_2O (δD = 0‰) calculated by combining published calibrations for $H_2(g)/H_2O(g)$, $H_2O(g)/H_2O(l)$, and $CH_4(g)/H_2(g)$ (see Sec. 4.1). Note that measured values for δD of H_2O in fluids from Lost City are +2 to +7‰ (Proskurowski et al., 2006) and thus the equilibrium values for CH_4 and H_2 at Lost City are slightly (~5‰) higher than those indicated by the curves. Gray arrows near bottom of plot bracket the probable range of temperatures for closure of H_2–H_2O isotopic exchange. The bar at top represents the mean ± 1*s* of measured $\Delta^{13}CH_3D$ values and corresponding clumped isotopologue temperatures (310^{+53}_{-42} °C) reported in Table 1, and black arrows point to the range of δD values of $CH_4(g)$ in equilibrium with seawater at the temperatures indicated by $\Delta^{13}CH_3D$ data. At right is a histogram of the δD data.

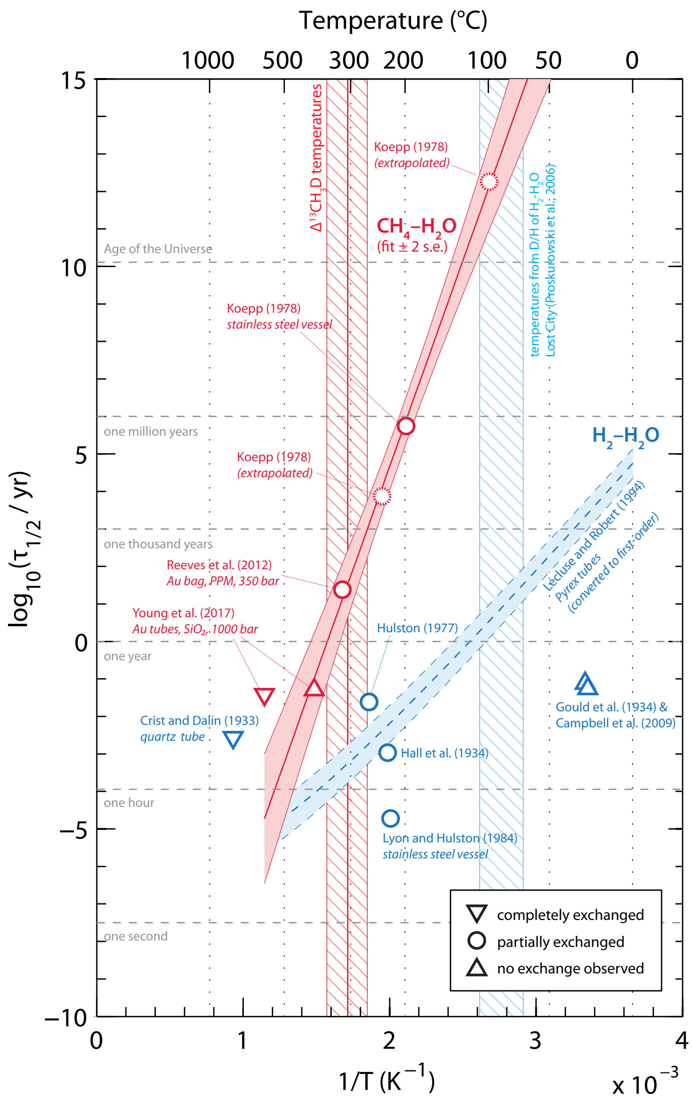

Fig. 4. Half-exchange timescales ($\tau_{1/2} = \ln(2) / k$) for hydrogen exchange between CH_4 & H_2O (red symbols) and H_2 & H_2O (blue) based on experiments done in the absence of added catalyst (Crist and Dalin, 1933; Hall et al., 1934; Gould et al., 1934; Hulston, 1977; Koepp, 1978; Lyon and Hulston, 1984; Lécluse and Robert, 1994; Campbell et al., 2009; Reeves et al., 2012; Young et al., 2017). Reactions were assumed to be first order in CH_4 or H_2. For data points representing experiments for which rate constants were not reported or in which exchange was not observed, the *y*-axis value is the duration of the experiment. Downward- and upward-pointing triangles are, respectively, maximum and minimum estimates of the exchange timescale. The $\tau_{1/2}$ for CH_4–H_2O exchange from Reeves et al. (2012) comes from Supplementary Fig. 1. Second-order rate coefficients for H_2–H_2O exchange from Lécluse and Robert (1994) were converted to pseudo-first-order rate coefficients by multiplying by the vapor pressure of H_2O calculated at temperatures T and a pressure of 1 kbar (see Sec. 4.1). Uncertainties in exchange rates are difficult to estimate, but are probably several orders of magnitude. Clumped isotopologue temperatures for CH_4 from the present study (red hatched bar) and apparent temperatures from D/H geothermometry of H_2–H_2O in endmember fluids at the Lost City site (blue hatched bar) (Proskurowski et al., 2006) are also shown.

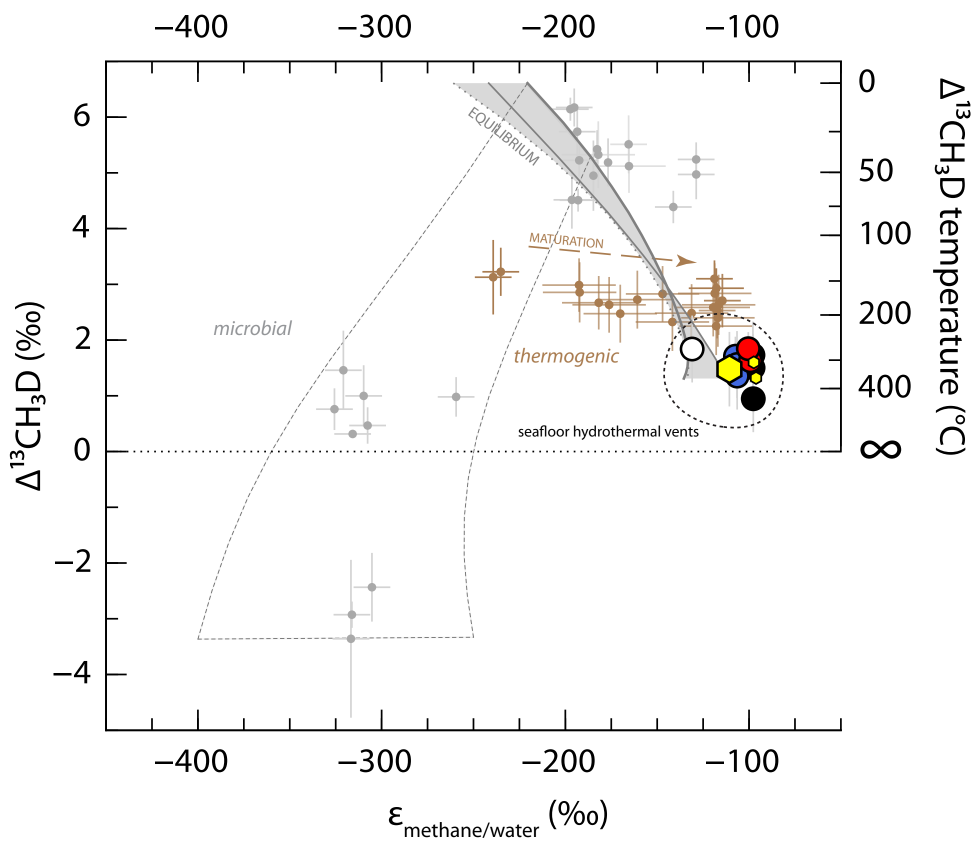

Fig. 5. Extents of (dis)equilibria in Reactions 1 and 2 in nature. The parameter on the *x*-axis represents the hydrogen-isotope fractionation between CH_4 and H_2O, and is defined: $\varepsilon_{methane/water} = \frac{(D/H)_{methane}}{(D/H)_{water}} - 1 = \frac{\delta D_{methane}+1}{\delta D_{water}+1} - 1$. Values of $\varepsilon_{methane/water}$ are identical to δD values of CH_4 when δD of H_2O is 0‰ (Fig. 3). Large symbols represent vent fluids from this study (symbols are the same as in Fig. 1), with the exception of the yellow octagons, which represent previously-reported data on hydrothermal fluids influenced by sedimentary-sourced thermogenic methane at Guaymas Basin (large octagon; Wang et al., 2015), and Main Endeavour field on the Juan de Fuca Ridge (small octagons; Douglas et al., 2017). Data shown as small circles are from Stolper et al. (2014), Inagaki et al. (2015), and Wang et al. (2015). The Δ_{18} data from Stolper et al. (2014) and Douglas et al. (2017) were converted to $\Delta^{13}CH_3D$ values (*y*-axis) following Wang (2017). Their position along the *x*-axis was estimated from literature data on δD of co-existing waters (either formation water or hot-spring water). Several other papers (Stolper et al., 2015; Douglas et al., 2016) reported values of Δ_{18} paired with $\varepsilon_{methane/water}$ data. These are not shown because of an irresolvable uncertainty in the conversion from values of Δ_{18} that do not reflect equilibrium to values of $\Delta^{13}CH_3D$ (see Wang, 2017).

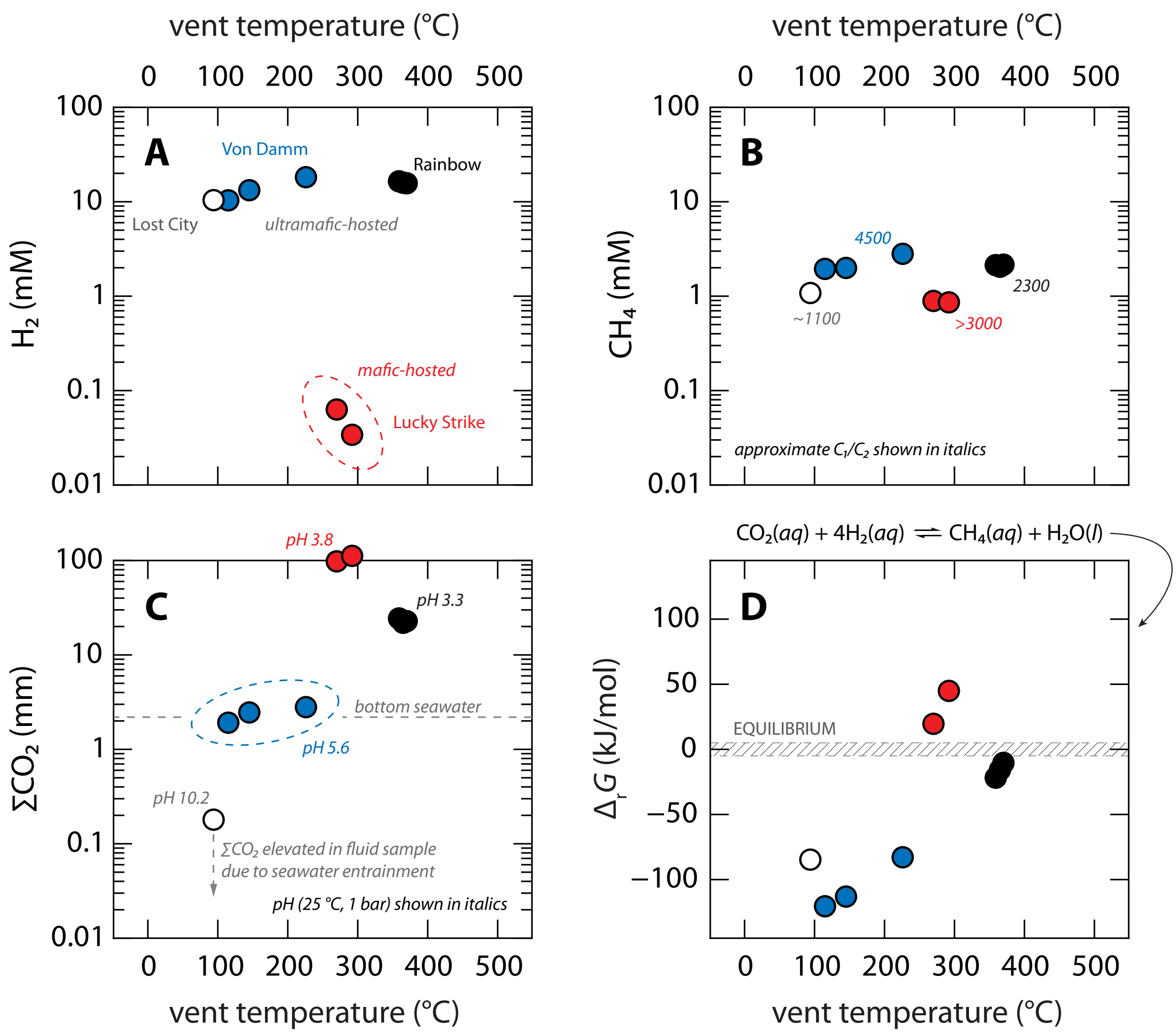

Fig. 6. Composition of vent fluids and energetics of methane synthesis in aqueous phase. Concentrations of (**A**) H_2, (**B**) CH_4, and (**C**) $\sum CO_2$ are plotted against measured vent temperatures (data from Table 2). Also shown are molar ratios of methane to ethane (C_1/C_2) in (B), and pH values of endmember fluids in (C). (**D**) Gibbs energy of reaction for methane formation from CO_2 and H_2 in aqueous solution (Reaction 5), calculated at vent T and P conditions ($\Delta_r G$, Table 2). Gray hatching represents thermodynamic equilibrium (taken as $\Delta_r G = 0 \pm 5$ kJ/mol). Methane formation in aqueous solution is thermodynamically favorable for points plotting below the hatched area. Symbol colors are the same as those in Fig. 1.

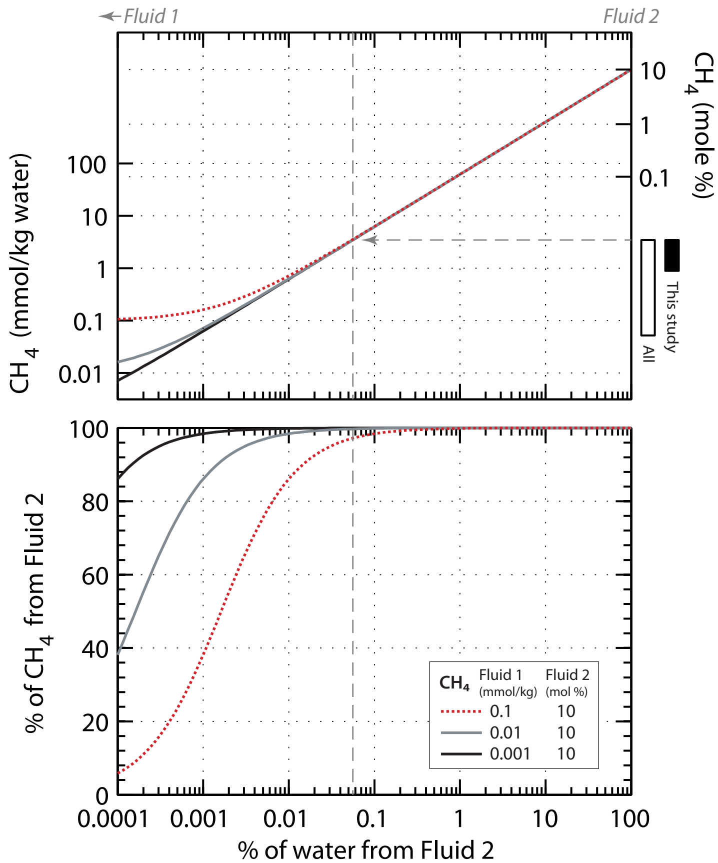

Fig. 7. Composition of fluids formed by mixing of a CH_4-poor actively-circulating seawater-derived hydrothermal fluid (*Fluid 1*) with a CH_4-rich fluid such as those observed in inclusions in plutonic rocks on the Southwest Indian Ridge and on the Mid-Atlantic Ridge (*Fluid 2*) (Kelley, 1996; Kelley, 1997; Kelley and Früh-Green, 1999). Mixing curves are plotted for CH_4 concentrations in the *Fluid 1* endmember ranging from 1 to 100 µmol/kg (assumed values for background CH_4 that is e.g., possible to be derived from complete thermal alteration of dissolved organic matter in deep ocean water). Calculations assume that molalities of species other than CH_4 have a negligible effect on mole fractions in the high-CH_4 fluid. The black and white bars show CH_4 concentrations in vent fluids from this study (Table 2) and from mid-ocean ridge hydrothermal systems globally (Keir, 2010).

9. TABLES

Table 1

Carbon and hydrogen isotope ratios and clumped isotopologue abundances of methane in studied hydrothermal fluids.

Field	Vent	Sample(s)	$\delta^{13}C$ (‰)	δD (‰)	$\Delta^{13}CH_3D$ (‰)		T_{13D} (°C)	
Rainbow	Guillaume	J2-352-IGT4	−17.6	−97.7	**0.95**	± 0.60	**450**	+298/−136
	CMSP&P	J2-354-IGT3	−17.5	−97.8	**1.50**	± 0.60	**322**	+142/−85
	Auberge	J2-352-IGT3	−17.4	−97.9	**1.73**	± 0.60	**285**	+114/−73
Von Damm	Old Man Tree[a]	J2-612-IGT6/-IGT8	−16.2	−107.4	**1.71**	± 0.35	**288**	+60/−47
	Ravelin 1	J2-617-IGT6	−16.4	−106.6	**1.56**	± 0.60	**312**	+134/−82
	East Summit	J2-612-IGT2	−16.4	−106.5	**1.35**	± 0.60	**350**	+167/−95
Lost City	Beehive	J2-361-IGT5/-CGTWu	−10.9	−126.6	**1.84**	± 0.60	**270**	+104/−68
Lucky Strike	Medea[a]	J2-359-IGT2/-CGTY	−14.2	−99.3	**1.63**	± 0.40	**301**	+75/−55
	Isabel[a]	J2-357-IGT5/-CGTY	−12.6	−100.4	**1.85**	± 0.30	**269**	+45/−37

Values for $\delta^{13}C$, δD, and $\Delta^{13}CH_3D$ are reported relative to Vienna Pee Dee Belemnite (VPDB), Vienna Standard Mean Ocean Water (VSMOW), and the stochastic distribution, respectively. Analytical uncertainties for $\delta^{13}C$ and δD are both ca. ±0.1‰ (95% confidence intervals). Uncertainties listed for $\Delta^{13}CH_3D$ and T_{13D} are 95% confidence intervals; the last digit in each (hundredths and ones places, respectively) is not significant.

[a] Samples analyzed in duplicate. Uncertainties listed are 2 s.e.m. (standard error of the mean) of the replicate measurements (n = 2).

Table 2

Fluid compositions[a] used in thermodynamic calculations and calculated Gibbs energy of reaction ($\Delta_r G$) for abiotic methane formation via Reaction 5 at studied vent sites.[b]

Field	Vent	T (°C)[c]	P (bar)	pH[d]	$\sum CO_2$ (mm)	H_2 (mM)	CH_4 (mM)	$\Delta_r G$ (kJ/mol)[e]
Rainbow	Guillaume	361	230	3.33	24.3	16.5	2.13	−22
	CMSP&P	365	230	3.36	21.9	15.9	2.05	−16
	Auberge	370	230	3.35	22.8	15.7	2.16	−11
Von Damm	Old Man Tree[f]	115	235	5.81	1.80	10.5	1.97	−121
	Ravelin 1[f]	145	235	5.83	2.52	13.4	2.02	−113
	East Summit	226	235	5.56	2.80	18.2	2.81	−83
Lost City	Beehive	96	70	10.20	0.18[g]	10.4	1.08	−85
Lucky Strike	Medea	270	170	3.81	98.0	0.063	0.89	+20
	Isabel	292	170	3.81	112.0	0.034	0.86	+45

Analytical uncertainties (2s) are ±2 °C for T; ±5% for H_2, $\sum CO_2$, and CH_4; and ±0.05 units for pH. Abbreviations: mm, mmol/kg fluid; mM, mmol/L fluid.

[a] All concentrations shown are extrapolated to endmember fluid composition (regressed to zero Mg content), except where noted. Data are from McDermott et al. (2015) and Reeves et al. (2014).

[b] For each vent fluid, the energetic favorability of methane formation was assessed by calculating the Gibbs energy of reaction ($\Delta_r G$), defined by the relationship: $\Delta_r G = RT \ln(Q/K)$, where R is the universal gas constant, T is measured fluid temperature in kelvin, Q is the reaction quotient, and K is the equilibrium constant at T and seafloor pressure P. Equilibrium constants were calculated using thermodynamic data and standard states from Johnson et al. (1992) and Shock and Helgeson (1990). For all calculations, the activity of $H_2O(l)$ was assumed to be unity. Activity coefficients were assumed to be unity for neutral dissolved species. For all fluids except for that from Lost City,[g] the concentration of $CO_2(aq)$ was assumed to be equal to $\sum CO_2$, a reasonable approximation given the low measured shipboard pH values and calculated equilibrium speciation of dissolved carbonate species at in-situ temperatures and seafloor pressures.

[c] Maximum measured vent temperature.

[d] Shipboard pH measurement (25 °C and 1 atm).

[e] A negative value of $\Delta_r G$ indicates a thermodynamic drive for the reaction to proceed as written from left to right (i.e., methane formation favored). Given uncertainties associated with chemical analyses and thermodynamic data, calculated $\Delta_r G$ values within ±5 kJ/mol of zero are interpreted to indicate that the reaction has approached or attained a state of thermodynamic equilibrium (Seewald, 2001).

[f] Concentrations for the fluids from Old Man Tree and Ravelin 1 vents at Von Damm were not extrapolated to zero Mg. Consistent high magnesium contents in duplicate gas-tight samples (14.0 and 15.0 mmol/kg fluid, respectively) indicate that fluids of the hot-spring source had mixed with seawater near the surface prior to discharge (McDermott et al., 2015), so they are not true zero-Mg endmembers. While CH_4 concentrations are lower in these fluids than in the Mg-deficient fluid from East Summit, ratios of CH_4 isotopologues did not change during subsurface mixing (Table 1).

[g] An arbitrary $CO_2(aq)$ concentration of 1 nmol/kg was used in thermodynamic calculations for the Lost City fluid, similar to Reeves et al. (2014). The actual concentration value is subject to substantial uncertainty due to difficulties in determining the near-zero endmember $\sum CO_2$ content in vent fluids, given that some entrainment of $\sum CO_2$-replete seawater always occurs during sampling (Proskurowski et al., 2008). Varying this value by as much as ten orders of magnitude would not affect the conclusion that methane formation is thermodynamically favorable in the fluid, due to the high H_2 content and the power of 4 to which the activity of $H_2(aq)$ is raised in the mass action expression.

Supplementary material for:

Clumped isotopologue constraints on the origin of methane at seafloor hot springs

Submitted to *Geochimica et Cosmochimica Acta* on 16 August 2017, revised 12 November 2017.

Authors and affiliations:

David T. Wang[a,b,]*, Eoghan P. Reeves[a,b,c], Jill M. McDermott[a,b,d], Jeffrey S. Seewald[b], and Shuhei Ono[a]

[a]Department of Earth, Atmospheric and Planetary Sciences, Massachusetts Institute of Technology, Cambridge, Massachusetts 02139, USA.
[b]Marine Chemistry and Geochemistry Department, Woods Hole Oceanographic Institution, Woods Hole, Massachusetts 02543, USA.
[c]Department of Earth Science and Centre for Geobiology, University of Bergen, Bergen N-5020, Norway.
[d]Earth and Environmental Sciences Department, Lehigh University, Bethlehem, Pennsylvania 18015, USA.

* Corresponding author. *E-mail address*: dtw@alum.mit.edu (D.T. Wang).

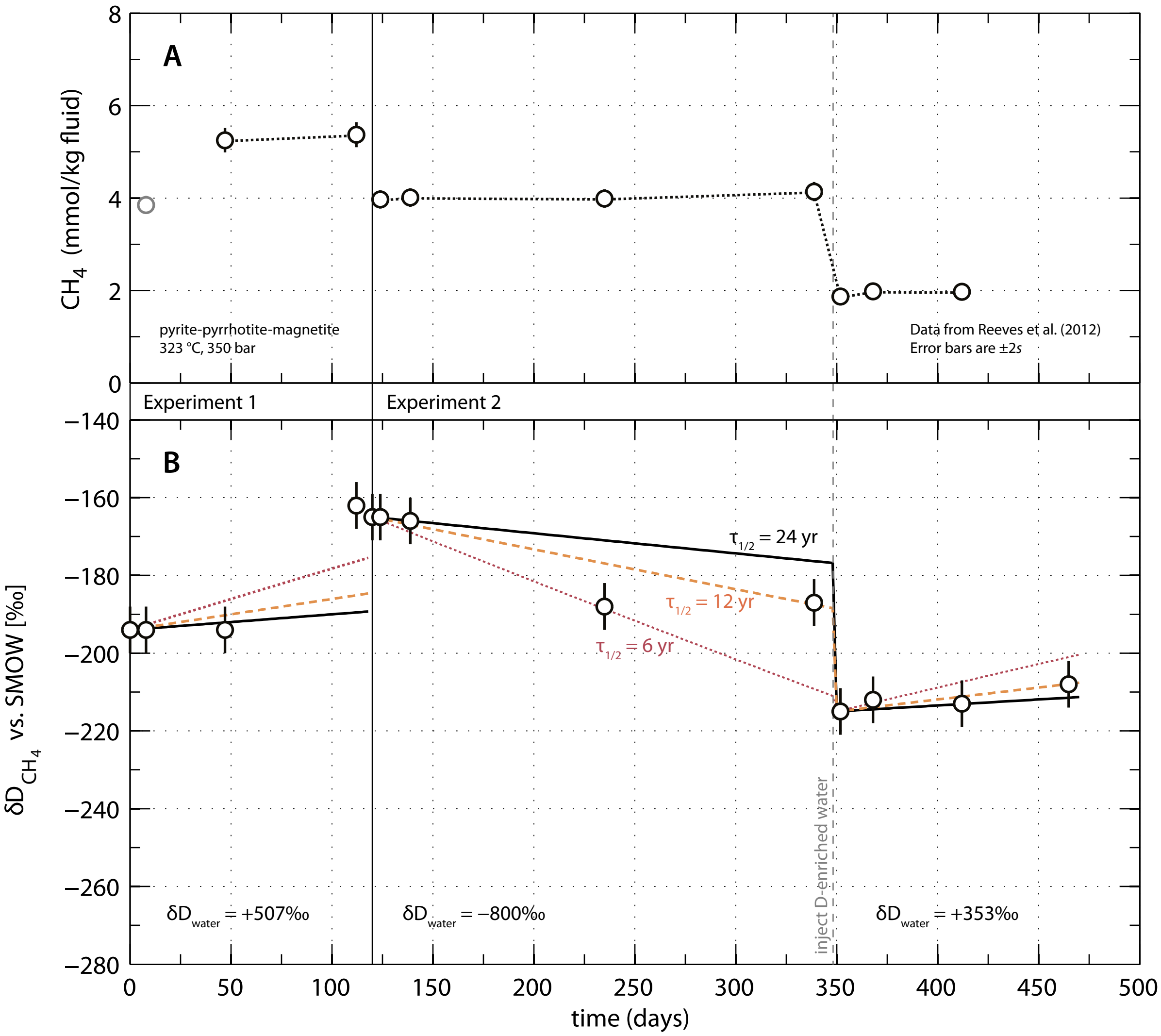

Supplementary Fig. 1. Experimental constraints on hydrogen exchange between CH_4(*aq*) and H_2O(*l*) from two experiments conducted by Reeves et al. (2012) in a flexible cell hydrothermal apparatus (gold-titanium oxide) at 323 °C and 350 bar. Concentrations of CH_4 (**A**) remain indistinguishable within analytical error (±5%, 2*s*) in Experiments 1 and 2. In Experiment 1, hydrocarbon concentrations in the first timepoint (8 days, shown in gray) were considered erroneously low, and can be excluded (see Reeves et al., 2012 for further details). Measured pH was ~4.2, and concentrations of H_2 and $\sum H_2S$ were 0.26–0.7 mmol/kg fluid and ~11 mmol/kg fluid, respectively, consistent with predictions for a Fe–S–O–H aqueous fluid buffered by pyrite-pyrrhotite-magnetite (PPM) at experimental conditions (Reeves et al., 2012). Panel (**B**) shows measurements of D/H of CH_4 compared against modeled kinetics for D/H exchange with varying half-exchange time ($\tau_{1/2} = \ln(2) / k$). The modeled kinetics assume that CH_4 concentration is constant, the rate of isotopic exchange is first order in CH_4, and the equilibrium D/H fractionation factor $[(D/H)_{methane}/(D/H)_{water} - 1]$ is −130‰ (see Figs. 3 and 5). We take $\tau_{1/2}$ = 24 yr (black curve) as a best-guess estimate of the rate of true isotopic exchange; this value is shown in Fig. 4.

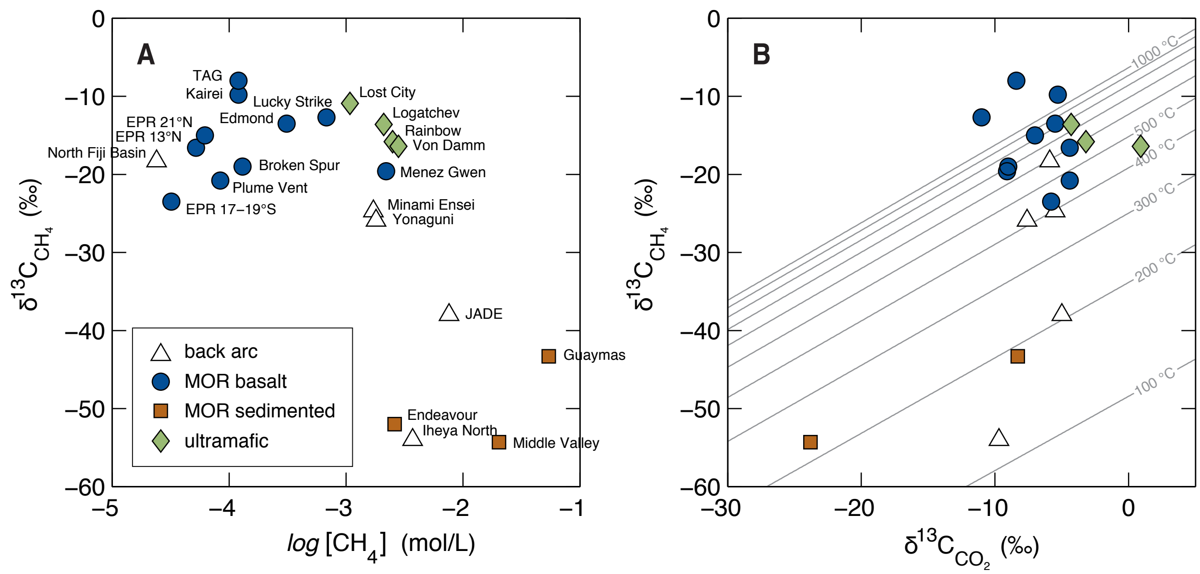

Supplementary Fig. 2. Carbon isotope data for CH_4 plotted against (**A**) CH_4 concentration and (**B**) $\delta^{13}C$ of inorganic carbon. Data from both sediment-influenced and unsedimented vent fields are shown. Data are from Charlou et al. (2000), Charlou et al. (2002), Cruse and Seewald (2006), Ishibashi et al. (1995), Charlou et al. (1996), Ishibashi et al. (1994), Kawagucci et al. (2011), Kumagai et al. (2008), Merlivat et al. (1987), Lein et al. (2000), Lilley et al. (1993), McDermott et al. (2015), Proskurowski et al. (2006), Proskurowski et al. (2008), Reeves et al. (2014), McCollom (2008), Konno et al. (2006), Welhan and Craig (1983), Welhan and Lupton (1987) and Evans et al. (1988). The curves in (B) are isotherms that represent carbon-isotopic equilibrium via the reaction: $^{12}CH_4(g) + {}^{13}CO_2(g) \rightleftharpoons {}^{13}CH_4(g) + {}^{12}CO_2(g)$ (Horita, 2001).

Supplementary Table 1

Measurements of methane samples tested for QA/QC. Each line in the table represents a ~1 cm^3 SATP quantity of CH_4 that was purified and analyzed in the same manner as the vent fluid samples reported in Table 1.

Sample	Sample(s)	$\delta^{13}C$ (‰)	δD (‰)	$\Delta^{13}CH_3D$ (‰)	T_{13D} (°C)
AL1[a]	PRAC-1 + PRAC-5[c]	−35.0	−149.9	**2.38** ± 0.29	**207** +31/−27
	PRAC-2 + PRAC-3[c]	−34.6	−147.1	**2.16** ± 0.40	**230** +51/−40
	PRAC-4	−33.8	−146.6	**2.26** ± 0.26	**220** +29/−25
NGS-3[b]	Hydrothermal Test	−73.5	−176.2	**5.33** ± 0.49	**39** +18/−16

Values for $\delta^{13}C$, δD, and $\Delta^{13}CH_3D$ are reported relative to Vienna Pee Dee Belemnite (VPDB), Vienna Standard Mean Ocean Water (VSMOW), and the stochastic distribution, respectively. Analytical uncertainties for $\delta^{13}C$ and δD are both ca. ±0.1‰ (95% confidence intervals). Uncertainties listed for $\Delta^{13}CH_3D$ and T_{13D} are 95% confidence intervals; the last digit in each (hundredths and ones places, respectively) is not significant.

[a] Accepted values of $\delta^{13}C$, δD, $\Delta^{13}CH_3D$, and T_{13D} of AL1 are −34.5‰, −147.7‰, +2.41 ± 0.07‰, and 204 ± 7 °C (95% confidence intervals), respectively (Wang, 2017).
[b] NGS-3 was determined in triplicate by Wang et al. (2015). The average of their reported values for $\delta^{13}C$, δD, $\Delta^{13}CH_3D$, and T_{13D} are −72.84 ± 0.08‰, −176.04 ± 0.23‰, +5.13 ± 0.06‰, and 46 ± 2 °C (95% confidence intervals), respectively.
[c] These are small aliquots of AL1 (~0.2 to 0.8 cm^3 SATP CH_4) that were prepared in separate serum bottles and pooled during purification prior to analysis. This was done to verify that our pooling procedure maintains isotopic integrity.

Supplementary Table 2

Compilation of hydrogen isotope ratios of CH_4 and H_2 and associated data on vent fluids from unsedimented hydrothermal systems.

Field	Vent[a]	T_{max} (°C)[b]	Mg (mM)[c]	$\sum CO_2$ (mm)	H_2 (mM)	CH_4 (mM)	$\delta^{13}C$ (‰)		δD (‰)			Notes
							$\sum CO_2$	CH_4	CH_4	H_2	H_2O[d]	
Mid-Atlantic Ridge												
Rainbow	Guillaume (X4)	361	0*	24.3	16.5	2.13	—	−17.6	−98	—	—	(1, 2)
	CMSP&P	365	0*	21.9	15.9	2.05	—	−17.5	−98	—	—	(1, 2)
	Auberge (X3)	370	0*	22.8	15.7	2.16	—	−17.4	−98	—	—	(1, 2)
	—	365	0*	16	16	2.5	−3.2[e]	−17.7	−105	−356	—	(3)
	—	360	0*	17	13	1.6	−2.5[e]	−17.8	−107	−379	—	(3)
Lost City	Beehive	94	0*	0.18	10.4	1.08	—	−10.9	−127	—	—	(1, 2)
		90	0*	—	—	—	—	—	−127	−609	+2 to 7	(4)
		90	0*	—	—	—	—	—	−126	−609	+2 to 7	(4)
	Marker 6	67	0*	—	—	—	—	—	−108	−605	+2 to 7	(4); cf. T_{max} 96 °C in ref. 2
		62	0*	—	—	—	—	—	−129	−616	+2 to 7	(4); cf. T_{max} 96 °C in ref. 2
	IMAX (IF)	55	—	—	—	—	—	—	−129	−649	+2 to 7	(4)
		55	—	—	—	—	—	—	−139	−646	+2 to 7	(4)
		55	—	—	—	—	—	—	−136	−648	+2 to 7	(4)
	Marker 7	28	—	—	—	—	—	—	−129	−663	+2 to 7	(4)
		28	—	—	—	—	—	—	−125	−666	+2 to 7	(4)
	Marker 8	43	—	—	—	—	—	—	−141	−658	+2 to 7	(4)
		43	—	—	—	—	—	—	−136	−651	+2 to 7	(4)
	Marker C	62	—	—	—	—	—	—	−126	−620	+2 to 7	(4)
		70	—	—	—	—	—	—	−130	−614	+2 to 7	(4)
	Marker H	60	—	—	—	—	—	—	−99	−657	+2 to 7	(4)
		60	—	—	—	—	—	—	−104	−689	+2 to 7	(4)
	Marker 3	61	—	—	—	—	—	—	−112	−610	+2 to 7	(4)
		71	—	—	—	—	—	—	−103	−605	+2 to 7	(4)
		73	—	—	—	—	—	—	−125	−609	+2 to 7	(4)
	—	93	0*	—	—	—	—	−11.9	−130	−618	—	(3)
Broken Spur	—	353	0*	—	—	—	—	—	—	−393	—	(4)
Logatchev	—	350	0*	—	—	—	—	—	−109	−372	—	(4); Logatchev 1?
Logatchev 1	—	346	0*	3.6	9	2.0	+4.1[e]	−10.2	−104	−350	—	(3)
	—	352	0*	4.4	13	2.6	+7.4[e]	−10.3	−104	−360	—	(3)
Logatchev 2	—	320	0*	6.2	11	1.2	+9.5[e]	−6.1	−93	−231	—	(3); phase-separated[f]
Ashadze 1	—	353	0*	3.7	8	0.5	+2.1[e]	−12.3	−104	−333	—	(3)
	—	353	0*	—	19	1.2	+4.6[e]	−14.1	−101	−343	—	(3)
Ashadze 2	—	296	0*	—	26	0.8	+0.2[e]	−8.7	−107	−270	—	(3); phase-separated[f]
Lucky Strike	Medea	270	0*	98	0.063	0.89	—	−14.2	−99	—	—	(1, 2)
	Isabel	292	0*	112	0.034	0.86	—	−12.6	−100	—	—	(1, 2)

Field	Vent[a]	T_{max}	Mg	$\sum CO_2$	H_2	CH_4	$\delta^{13}C$ (‰)		δD (‰)			Notes
		(°C)[b]	(mM)[c]	(mm)	(mM)	(mM)	$\sum CO_2$	CH_4	CH_4	H_2	H_2O[d]	
East Pacific Rise												
9° N	—	380	0*	—	—	—	—	—	—	−328	—	(4)
21° N	Nat. Geo. Soc.	350	0*	—	30.5	1.4	−7.0	−15.0	−102	−401	+0.5	(5, 6)
Central Indian Ridge												
Kairei	Kali	362	0*	8.0	3.3	0.12	−5.3	−9.8	—	−368	—	(7, 8)
		316	8.4	12.1	3.6	—	—	—	—	−328	—	(7, 8)
	Monju	299	5.2	7.9	2.1	—	—	—	—	−385	—	(7, 8)
		42	50.9	9.3	$8{\times}10^{-4}$	—	—	—	—	−431	—	(7, 8)
		87	43.7	6.0	0.69	—	—	—	—	−361	—	(7, 8); snail colony[f]
		22	48.3	12.6	0.13	—	—	—	—	−493	—	(7, 8); snail colony[f]
	Fugen	305	4.5	9.5	2.7	—	—	—	—	−391	—	(7, 8)
	Daikoku (Marker 30)	306	0*	—	2.2	—	—	—	—	−340	—	(7)
	—	350	0*	—	—	—	—	—	—	−400	—	(4)
Edmond	Nura Nura	375	0*	12.8	0.11	0.31	−5.5	−13.5	—	−362	—	(7, 8)
	Marker 27	325	0*	12.3	0.10	—	—	—	—	−377	—	(7, 8)
	White Head	263	12.4	8.1	0.04	—	—	—	—	−412	—	(7, 8)
	Grand Shrimp Valley	281	13.4	12.1	0.48	—	—	—	—	−681	—	(7, 8); shrimp colony[f]
	Marker 24	116	40.6	8.7	0.07	—	—	—	—	−476	—	(7, 8)
Mid-Cayman Rise												
Von Damm	Old Man Tree	115	14.0	1.80	10.5	1.97	—	−16.2	−107	—	—	(1, 9)
	Ravelin 1	145	15.0	2.52	13.4	2.02	—	−16.4	−107	—	—	(1, 9)
	East Summit	226	0*	2.80	18.2	2.81	—	−16.4	−107	—	—	(1, 9)

Data sources: (1) this study; (2) Reeves et al. (2014); (3) Charlou et al. (2010); (4) Proskurowski et al. (2006); (5) Welhan and Craig (1983); (6) Horibe and Craig (1995); (7) Kawagucci et al. (2010); (8) Kumagai et al. (2008); (9) McDermott et al. (2015).

Abbreviations: mm, mmol/kg fluid; mM, mmol/L fluid.

[a] Dash (—) indicates that data were not reported or that samples were unable to be matched across multiple references.
[b] Maximum measured vent temperature.
[c] Asterisk (*) indicates near-endmember fluid sample (represented by stars in Fig. 4). For these samples, concentrations of $\sum CO_2$, H_2, and CH_4 and $\delta^{13}C$ values of $\sum CO_2$ have been extrapolated to endmember fluid composition (regressed to zero Mg content) assuming entrainment of seawater containing ~53 mM Mg.
[d] Endmember vent fluids typically have δD values of H_2O between −2 and +4‰ (Shanks et al., 1995). A value of 0‰ was assumed when no data could be found (see text and Fig. 4).
[e] Values are as reported; it is not known whether correction for $\sum CO_2$ in seawater was applied.
[f] Figure 4 excludes data from these fluids, which have either effluxed through macrofaunal colonies or are venting with atypically low salinity.

References Cited in Supplement

Charlou J., Donval J., Douville E., Jean-Baptiste P., Radford-Knoery J., Fouquet Y., Dapoigny A. and Stievenard M. (2000) Compared geochemical signatures and the evolution of Menez Gwen (37 50 N) and Lucky Strike (37 17 N) hydrothermal fluids, south of the Azores Triple Junction on the Mid-Atlantic Ridge. *Chemical Geology* **171**, 49–75.

Charlou J., Donval J., Fouquet Y., Jean-Baptiste P. and Holm N. (2002) Geochemistry of high H_2 and CH_4 vent fluids issuing from ultramafic rocks at the Rainbow hydrothermal field (36 14 N, MAR). *Chemical Geology* **191**, 345–359.

Charlou J. L., Fouquet Y., Donval J. P., Auzende J. M., Jean-Baptiste P., Stievenard M. and Michel S. (1996) Mineral and gas chemistry of hydrothermal fluids on an ultrafast spreading ridge: East Pacific Rise, 17° to 19°S (Naudur cruise, 1993) phase separation processes controlled by volcanic and tectonic activity. *Journal of Geophysical Research: Solid Earth* **101**, 15899–15919.

Charlou J. L., Donval J. P., Konn C., Ondréas H., Fouquet Y., Jean-Baptiste P. and Fourré E. (2010) High production and fluxes of H_2 and CH_4 and evidence of abiotic hydrocarbon synthesis by serpentinization in ultramafic-hosted hydrothermal systems on the Mid-Atlantic Ridge. *Diversity of Hydrothermal Systems on Slow Spreading Ocean Ridges*, 265–296.

Cruse A. M. and Seewald J. S. (2006) Geochemistry of low-molecular weight hydrocarbons in hydrothermal fluids from Middle Valley, northern Juan de Fuca Ridge. *Geochimica et Cosmochimica Acta* **70**, 2073–2092.

Evans W. C., White L. D. and Rapp J. B. (1988) Geochemistry of some gases in hydrothermal fluids from the southern Juan de Fuca Ridge. *Journal of Geophysical Research: Solid Earth* **93**, 15305–15313.

Horibe Y. and Craig H. (1995) D/H fractionation in the system methane-hydrogen-water. *Geochimica et Cosmochimica Acta* **59**, 5209–5217.

Horita J. (2001) Carbon isotope exchange in the system CO_2–CH_4 at elevated temperatures. *Geochimica et Cosmochimica Acta* **65**, 1907–1919.

Ishibashi J., Sano Y., Wakita H., Gamo T., Tsutsumi M. and Sakai H. (1995) Helium and carbon geochemistry of hydrothermal fluids from the Mid-Okinawa Trough Back Arc Basin, southwest of Japan. *Chemical Geology* **123**, 1–15.

Ishibashi J.-I., Wakita H., Nojiri Y., Grimaud D., Jean-Baptiste P., Gamo T., Auzende J.-M. and Urabe T. (1994) Helium and carbon geochemistry of hydrothermal fluids from the North Fiji Basin spreading ridge (southwest Pacific). *Earth and Planetary Science Letters* **128**, 183–197.

Kawagucci S., Toki T., Ishibashi J., Takai K., Ito M., Oomori T. and Gamo T. (2010) Isotopic variation of molecular hydrogen in 20°–375°C hydrothermal fluids as detected by a new analytical method. *Journal of Geophysical Research: Biogeosciences* **115**, G03021.

Kawagucci S., Chiba H., Ishibashi J., Yamanaka T., Toki T., Muramatsu Y., Ueno Y., Makabe A., Inoue K., Yoshida N., Nakagawa S., Nunoura T., Takai K., Takahata N., Sano Y., Narita T., Teranishi G., Obata H. and Gamo T. (2011) Hydrothermal fluid geochemistry at the Iheya North field in the mid-Okinawa Trough: Implication for origin of methane in subseafloor fluid circulation systems. *Geochemical Journal* **45**, 109–124.

Konno U., Tsunogai U., Nakagawa F., Nakaseama M., Ishibashi J., Nunoura T. and Nakamura K. (2006) Liquid CO_2 venting on the seafloor: Yonaguni Knoll IV hydrothermal system, Okinawa Trough. *Geophysical Research Letters* **33**.

Kumagai H., Nakamura K., Toki T., Morishita T., Okino K., Ishibashi J., Tsunogai U., Kawagucci S., Gamo T., Shibuya T., Sawaguchi T., Neo N., Joshima M., Sato T. and Takai K. (2008) Geological background of the Kairei and Edmond hydrothermal fields along the Central Indian Ridge: implications of their vent fluids' distinct chemistry. *Geofluids* **8**, 239–251.

Lein A. Y., Grichuk D., Gurvich E. and Bogdanov Y. A. (2000) A new type of hydrogen-and methane-rich hydrothermal solutions in the Rift zone of the Mid-Atlantic Ridge. *Doklady Earth Sciences* **375A**, 1391–1394.

Lilley M., Butterfield D., Olson E., Lupton J., Macko S. and McDuff R. (1993) Anomalous CH_4 and NH_4^+ concentrations at an unsedimented mid-ocean-ridge hydrothermal system. *Nature* **364**, 45–47.

McCollom T. M. (2008) Observational, experimental, and theoretical constraints on carbon cycling in mid-ocean ridge hydrothermal systems. In *Magma to Microbe: Modeling Hydrothermal Processes at Ocean Spreading Centers* American Geophysical Union. pp. 193–213.
McDermott J. M., Seewald J. S., German C. R. and Sylva S. P. (2015) Pathways for abiotic organic synthesis at submarine hydrothermal fields. *Proceedings of the National Academy of Sciences of the United States of America* **112**, 7668–7672.
Merlivat L., Pineau F. and Javoy M. (1987) Hydrothermal vent waters at 13°N on the East Pacific Rise: isotopic composition and gas concentration. *Earth and Planetary Science Letters* **84**, 100–108.
Proskurowski G., Lilley M. D., Kelley D. S. and Olson E. J. (2006) Low temperature volatile production at the Lost City Hydrothermal Field, evidence from a hydrogen stable isotope geothermometer. *Chemical Geology* **229**, 331–343.
Proskurowski G., Lilley M. D., Seewald J. S., Früh-Green G. L., Olson E. J., Lupton J. E., Sylva S. P. and Kelley D. S. (2008) Abiogenic hydrocarbon production at Lost City hydrothermal field. *Science* **319**, 604–607.
Reeves E. P., McDermott J. M. and Seewald J. S. (2014) The origin of methanethiol in midocean ridge hydrothermal fluids. *Proceedings of the National Academy of Sciences of the United States of America* **111**, 5474–5479.
Reeves E. P., Seewald J. S. and Sylva S. P. (2012) Hydrogen isotope exchange between *n*-alkanes and water under hydrothermal conditions. *Geochimica et Cosmochimica Acta* **77**, 582–599.
Shanks W. C., Böhlke J. K. and Seal R. R. (1995) Stable isotopes in mid-ocean ridge hydrothermal systems: interactions between fluids, minerals, and organisms. In *Seafloor Hydrothermal Systems: Physical, Chemical, Biological, and Geological Interactions* (eds. S. E. Humphris, R. A. Zierenberg, L. S. Mullineaux, and R. E. Thomson). American Geophysical Union. pp. 194–221.
Wang D. T. (2017) The geochemistry of methane isotopologues. Ph.D. thesis, Massachusetts Institute of Technology and Woods Hole Oceanographic Institution. doi:10.1575/1912/9052
Wang D. T., Gruen D. S., Lollar B. S., Hinrichs K.-U., Stewart L. C., Holden J. F., Hristov A. N., Pohlman J. W., Morrill P. L., Könneke M., Delwiche K. B., Reeves E. P., Sutcliffe C. N., Ritter D. J., Seewald J. S., McIntosh J. C., Hemond H. F., Kubo M. D., Cardace D., Hoehler T. M. and Ono S. (2015) Nonequilibrium clumped isotope signals in microbial methane. *Science* **348**, 428–431.
Welhan J. A. and Craig H. (1983) Methane, hydrogen and helium in hydrothermal fluids at 21°N on the East Pacific Rise. In *Hydrothermal Processes at Seafloor Spreading Centers* Springer. pp. 391–409.
Welhan J. and Lupton J. (1987) Light hydrocarbon gases in Guaymas Basin hydrothermal fluids: thermogenic versus abiogenic origin. *AAPG Bulletin* **71**, 215–223.